



# An optimised organic carbon / elemental carbon (OC / EC) fraction separation method for radiocarbon source apportionment applied to low-loaded Arctic aerosol filters

Martin Rauber<sup>1,2</sup>, Gary Salazar<sup>1,2</sup>, Karl Espen Yttri<sup>3</sup>, and Sönke Szidat<sup>1,2</sup>

<sup>1</sup>Department of Chemistry, Biochemistry and Pharmaceutical Sciences, University of Bern, Bern, Switzerland

<sup>2</sup>Oeschger Centre for Climate Change Research, University of Bern, Bern, Switzerland

<sup>3</sup>Department of Atmospheric and Climate Research, NILU – Norwegian Institute for Air Research, Kjeller, Norway

**Correspondence:** Sönke Szidat (soenke.szidat@unibe.ch)

Received: 12 July 2022 – Discussion started: 26 August 2022

Revised: 10 January 2023 – Accepted: 11 January 2023 – Published: 14 February 2023

**Abstract.** Radiocarbon ( $^{14}\text{C}$ ) analysis of carbonaceous aerosols is used for source apportionment, separating the carbon content into fossil vs. non-fossil origin, and is particularly useful when applied to subfractions of total carbon (TC), i.e. elemental carbon (EC), organic carbon (OC), water-soluble OC (WSOC), and water-insoluble OC (WINSOC). However, this requires an unbiased physical separation of these fractions, which is difficult to achieve. Separation of EC from OC using thermal–optical analysis (TOA) can cause EC loss during the OC removal step and form artificial EC from pyrolysis of OC (i.e. so-called charring), both distorting the  $^{14}\text{C}$  analysis of EC. Previous work has shown that water extraction reduces charring. Here, we apply a new combination of a WSOC extraction and  $^{14}\text{C}$  analysis method with an optimised OC/EC separation that is coupled with a novel approach of thermal-desorption modelling for compensation of EC losses. As water-soluble components promote the formation of pyrolytic carbon, water extraction was used to minimise the charring artefact of EC and the eluate subjected to chemical wet oxidation to  $\text{CO}_2$  before direct  $^{14}\text{C}$  analysis in a gas-accepting accelerator mass spectrometer (AMS). This approach was applied to 13 aerosol filter samples collected at the Arctic Zeppelin Observatory (Svalbard) in 2017 and 2018, covering all seasons, which bear challenges for a simplified  $^{14}\text{C}$  source apportionment due to their low loading and the large portion of pyrolysable species. Our approach provided a mean EC yield of  $0.87 \pm 0.07$  and reduced the charring to 6.5 % of the recovered EC amounts. The mean fraction modern ( $F^{14}\text{C}$ ) over all seasons was  $0.85 \pm 0.17$  for TC;  $0.61 \pm 0.17$  and  $0.66 \pm 0.16$  for EC be-

fore and after correction with the thermal-desorption model, respectively; and  $0.81 \pm 0.20$  for WSOC.

## 1 Introduction

Considerable efforts have been made to investigate atmospheric aerosol due to its relevance to a wide range of environmental topics, including change in radiative forcing and adverse effects on human health (McNeill, 2017; Lelieveld et al., 2015; Landrigan, 2017; Pope et al., 2020). Exposure to ambient atmospheric particulate matter (PM) has been associated with damage to the cardiopulmonary system and causing at least 3 million premature deaths per year globally (Kim et al., 2015; Lelieveld et al., 2015; GBD 2015 Risk Factors Collaborators, 2016). Understanding aerosols is therefore crucial for future projections and for the improvement of air quality, especially for severely affected areas (Quinn et al., 2008; Bond et al., 2013; Schmale et al., 2021). Although the Arctic is considered a pristine part of the world, it is also affected by emissions from polluted regions in the Northern Hemisphere, causing the Arctic haze phenomenon (Barrie, 1986; Heidam et al., 2004; Quinn et al., 2002; Zhao and Garrett, 2015; Engelmann et al., 2021; Jouan et al., 2014), occurring in late winter and early spring, and which have been known for decades (Barrie et al., 1981). Arctic haze consists mainly of sulfate and carbonaceous aerosols trapped in the cold retracting polar dome in spring, coupled with reduced

wet scavenging in winter and spring (Abbatt et al., 2019; Moschos et al., 2022).

Carbonaceous aerosols (here, total carbon, TC) consists of an organic fraction referred to as organic carbon (OC), and a refractory light-absorbing component named elemental carbon (EC) or equivalent black carbon (eBC) when quantified with thermal–optical analysis or optical methods, respectively (Contini et al., 2018; Bond et al., 2013; Petzold et al., 2013). TC constitutes 20 % to 90 % of the aerosol mass (Kanakidou et al., 2005; Putaud et al., 2010; Gentner et al., 2017). As a main PM component, it thus contributes to adverse effects on public health and climate. On the one hand, carbonaceous aerosols may contain toxic or carcinogenic compounds such as polycyclic aromatic hydrocarbons (PAHs) (Mauderly and Chow, 2008; Kim et al., 2013; Smichowski et al., 2005; Daellenbach et al., 2020). On the other hand, both EC and OC are climate relevant: the effective radiative forcing (ERF) for atmospheric aerosols is negative, and while the OC fraction has a negative ERF, the EC fraction has a positive ERF (IPCC, 2021). Overall, the surface albedo for black carbon (BC) and OC on snow and ice is positive with a global mean ERF of 0.08 (0.00 to 0.18) (IPCC, 2021). Consequently, sources of OC, EC, and subfractions must be understood to improve air quality and mitigate adverse effects of carbonaceous aerosols. Due to their complex composition and multitude of sources, however, carbonaceous aerosols are still inadequately understood.

Source apportionment is a widely used approach to gain understanding on the emission, formation, and transformation of carbonaceous aerosols. It investigates the chemical and physical composition of aerosols at receptor sites to disentangle the contributions of individual emissions and the attribution to different source categories. Radiocarbon ( $^{14}\text{C}$ ) measurements constitute an important source apportionment tool that can unambiguously separate between fossil and contemporary carbon present in carbonaceous aerosol, including in the OC and EC subfractions (Szidat et al., 2006; Winiger et al., 2015; Zotter et al., 2014). Sources of OC and EC are often very different, and such additional information is obtained by means of  $^{14}\text{C}$  source apportionment of both EC and OC compared to a radiocarbon of TC analysis alone. The analysis of the OC subfractions water-soluble OC (WSOC) and water-insoluble OC (WINSOC) can lead to further information on the fossil and non-fossil fractions of the emitting sources (Zhang et al., 2014b).

Separation of OC and EC is method dependent, but the classification is widely recognised (Pöschl, 2003). EC is a primary particle, i.e. emitted directly to the atmosphere and generated by incomplete combustion of fossil fuels and biomass, whereas OC is either primary or secondary, i.e. emitted directly or formed in the atmosphere by oxidation of both anthropogenic and biogenic precursor gases (Kanakidou et al., 2005). Thermal–optical analysis (TOA) is a well-established and commonly used technique for OC/EC determination (Chow et al., 2004; Cavalli et al., 2010; Chow

et al., 1993; Schmid et al., 2001; Huntzicker et al., 1982; Zenker et al., 2017; Dasari and Widory, 2022). Typically, two or more heating steps in an inert (i.e. helium) and in an oxidative atmosphere (i.e. 2 % oxygen in helium) are used to desorb OC and EC, respectively. During analysis, the transmission or reflectance of the filter sample is continuously measured (Birch and Cary, 1996; Schmid et al., 2001). A change in the transmission or reflectance signal indicates charring and EC loss. Charring is known as the process when OC pyrolyses and forms pyrolytic carbon (PC) that shows similar optical properties to EC, thus decreasing the transmission signal and creating a positive EC artefact (Cadle et al., 1980; Yu et al., 2002; Chow et al., 2004; Boparai et al., 2008). Charring leads to an overestimation of EC and an underestimation of OC. Additionally to charring, some EC is lost by desorption during thermal separation of OC, leading to a negative EC artefact. Both the positive EC artefact (i.e. charring) and the negative artefact (i.e. partial EC loss) may induce a bias in  $^{14}\text{C}$  measurement of EC. Charring adds OC, which is typically has a higher non-fossil proportion than EC (Szidat et al., 2006, 2009; Zhang et al., 2012, 2014b; Zotter et al., 2014; Vlachou et al., 2018), so that the measured  $^{14}\text{C}$  of EC may appear to have a higher non-fossil proportion than it does. Partial EC loss usually affects non-fossil EC (e.g. from biomass burning) more than fossil EC (e.g. from traffic or coal combustion) so that the remaining EC may be altered and seem to have a higher fossil proportion. Correction of both artefacts is therefore required for the accurate quantification of the fossil vs. non-fossil shares of EC. EC recovery after OC/EC separation is determined using the transmission or reflectance signal (Gundel et al., 1984; Zhang et al., 2012). Frequently used TOA protocols for OC/EC determination include EUSAAR\_2 (Cavalli et al., 2010), IMPROVE (Chow et al., 1993), and NIOSH (Eller and Cassinelli, 1996). Radiocarbon measurement requires a clear physical separation of OC and EC, since OC and EC do not originate from the same processes and often show very different radiocarbon signatures (Szidat et al., 2006, 2007; Zhang et al., 2014b). Traditional TOA protocols may still contain some OC in charred or an unaltered form after the split point and thus fail to perform the physical separation adequately for radiocarbon source apportionment (Barrett et al., 2015; Zhang et al., 2012). Gustafsson et al. (2001) developed a separation technique (CTO-375) in soil sediments, which was later applied to radiocarbon source apportionment of atmospheric aerosols (Zencak et al., 2007). A two-step separation method developed by Szidat et al. (2004b) was utilised for radiocarbon source apportionment (Zhang et al., 2010; Jenk et al., 2007; Szidat et al., 2004b). As these simplified approaches still failed to provide isolation of EC, our group (Zhang et al., 2012) established an improved four-step method (Swiss\_4S) that aimed at a best-possible congruence with existing TOA protocols (especially with EUSAAR\_2) and additionally used water extraction before TOA and pure  $\text{O}_2$  for an optimised EC recovery and reduced char-

ring. Nevertheless, the quantification of EC losses and PC formation remains a challenge, as both fractions and processes typically overlap each other and can hardly be distinguished from each other (Boparai et al., 2008). Later, Agrios et al. (2015) coupled the Sunset thermo-optical OC/EC analyser with online measurement in an accelerator mass spectrometer (AMS) and implemented the previously developed Swiss\_4S protocol.

Many have investigated EC in the Arctic including stable isotope ( $^{13}\text{C}$ ) and radiocarbon analysis for source apportionment (Winiger et al., 2016, 2017, 2015; Moschos et al., 2021). The fossil contribution of OC and WSOC is often not measured directly but calculated by the isotope mass balance approach (Vlachou et al., 2018). Zhang et al. (2014a) lyophilised and re-solubilised the eluate from water extraction before combustion in an elemental analyser coupled with radiocarbon measurement. Menzel and Vaccaro (1964) as well as Sharp (1973) used potassium persulfate for the oxidation of dissolved organic carbon in seawater. Lang et al. (2012) employed such a chemical wet oxidation for stable isotope analysis of dissolved organic matter in freshwater samples. This method was later used for stable and radiocarbon analysis of marine samples as well as compound-specific analysis of pyrogenic carbon (Lang et al., 2013; Wiedemeier et al., 2016), but it has not been adapted for  $^{14}\text{C}$  analysis of WSOC from carbonaceous aerosols so far.

The present study provides a framework for an optimal OC/EC separation and radiocarbon analysis coupled with direct  $^{14}\text{C}$ (WSOC) analysis (i.e. the  $^{14}\text{C}$  analysis of WSOC) by chemical wet oxidation applied on low-loaded Arctic filters. We provide a novel method for the EC yield extrapolation and charring correction based on a chemical desorption model that represents the behaviour of EC from different sources more realistically. Arctic filters were utilised as they are challenging for radiocarbon analysis due to their low loading and the large portion of pyrolysable species. Using an optimised strategy, we can measure the  $F^{14}\text{C}$  value (i.e. the fraction modern) in all major aerosol filter fractions (TC, EC, WSOC, WINSOC) with the lowest possible amount of filter material if sufficient filter loading is provided.

## 2 Experimental

### 2.1 Overview of the analytical procedures

Aerosol filter samples were first water-extracted to collect WSOC for subsequent radiocarbon measurement and to minimise formation of PC, caused primarily by WSOC, otherwise causing a dilution of the true  $^{14}\text{C}$ (EC) signal. We then used the first three steps of the Swiss\_4S protocol (Zhang et al., 2012) to remove WINSOC from the filter by thermal-optical analysis, isolating EC. The filter's EC content was evolved by total combustion in a TOA analyser and subjected to online radiocarbon measurements. The WSOC eluate was

converted to  $\text{CO}_2$  by chemical wet oxidation before radiocarbon measurement. The following sections explain the different procedures in brief, whereas the Supplement provides information that is more detailed.

### 2.2 Sampling and filter selection

Aerosol filter samples were collected between February 2017 and November 2018 at the Zeppelin Observatory (Svalbard) ( $78^\circ 54' \text{N}$ ,  $11^\circ 52' \text{E}$ ; 475 m a.s.l.), which is part of the Global Atmospheric Watch (GAW) programme, the Arctic Monitoring and Assessment Programme (AMAP), and the European Evaluation and Monitoring Programme (EMEP) (Hung et al., 2010; Tørseth et al., 2012; Platt et al., 2022). Aerosol particles were collected on pre-fired ( $850^\circ\text{C}$ , 3 h) quartz fibre filters (Pallflex<sup>®</sup> Tissuquartz 2500QAT-UP; 150 mm in diameter) downstream of a  $\text{PM}_{10}$  inlet, using a Digitel high-volume sampler (DH-77, Hegenau, Switzerland). The sampler operated at a flow rate of  $689 \text{ L min}^{-1}$ , corresponding to an air volume of  $6945 \text{ m}^3$  for a sampling time of 1 week. Filter samples were collected according to the quartz-behind-quartz (QBQ) setup (McDow and Huntzicker, 1990), allowing for an estimate of the positive sampling artefact of OC.

A fraction (46 mm diameter, corresponding to  $16.6 \text{ cm}^2$ ) of the total filter area ( $153.9 \text{ cm}^2$ ) were cut for radiocarbon measurement of  $^{14}\text{C}$ (TC),  $^{14}\text{C}$ (WSOC), and  $^{14}\text{C}$ (EC) (Fig. 1). The filter's TC, EC, and OC contents were quantified according to the EUSAAR\_2 temperature programme (Cavalli et al., 2010), using transmission for charring correction. A total of 18 filter samples were received for radiocarbon measurement, but due to low EC loadings, pooling of 5 subsequent filters was necessary (Fig. 1). Owing to the low filter loading, the water extraction for  $^{14}\text{C}$ (WSOC) and  $^{14}\text{C}$ (EC) was only performed on the front filters, whereas  $^{14}\text{C}$ (TC) analysis was performed on both front and back filters.

### 2.3 Water extraction

Three circular punches of 22 mm (diameter) made from the 46 mm (diameter) aerosol filter were stacked and intercalated with silicone O-rings in 25 mm polycarbonate filter holders (Sartorius GmbH, Germany) with the exposed side facing upwards. A cleaned glass syringe (10 mL, ETERNA MATIC, Sanitex SA, Switzerland) was rinsed and filled with ultrapure water ( $18.2 \text{ M}\Omega \text{ cm}$ , Elga Purelab flex 2, High Wycombe, UK) and attached to the filter holder with a  $21 \text{ G} \times 4.75 \text{ in.}$  needle (Sterican, B. Braun, Germany) at the filter holder outlet (Fig. 1). The needle pierced through a 12 mL EXETAINER<sup>®</sup> vial septum (12 mL, screw cap, item 938 W, Labco Ltd., Lampeter, UK). A total of  $5.0 \pm 0.2 \text{ mL}$  of water passed through the filters by gravity and collected in the EXETAINER<sup>®</sup> vials. Excess air could exit the vial by opening the screw cap half a turn before needle insertion. After water extraction, the vials were closed and stored at  $4^\circ\text{C}$  until WSOC measurement. Excess water in the filter holder

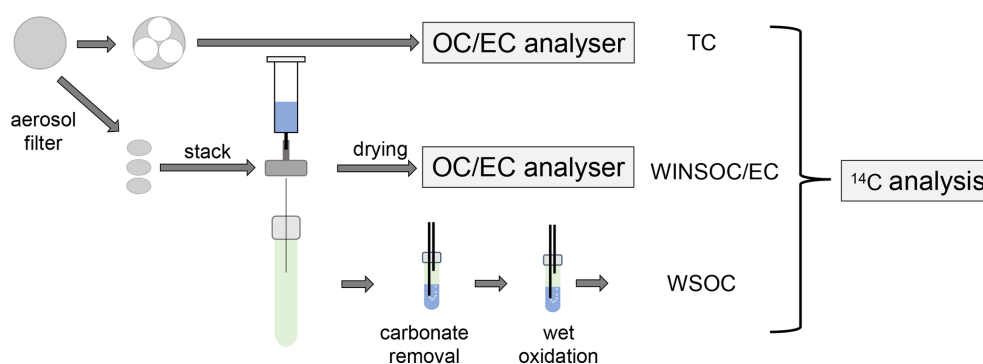


**Figure 1.** Separation of the different fractions for  $^{14}\text{C}$  analysis starting from the aerosol filters. One or multiple circular quartz fibre filter punches are stacked and intercalated in the water extraction setup. The residual filter material is used for WINSOC and EC analysis after drying, and the extract is oxidised by chemical wet oxidation. The remaining filter material is used for TC analysis.

was removed using low-lint tissues, and the water-extracted filters were dried overnight. The water-extracted area (18 mm diameter) of the filter disc was punched out to remove the circumference that was not extracted, wrapped in aluminium foil, packed in airtight plastic bags, and stored in a freezer at  $-20^\circ\text{C}$  for subsequent WINSOC removal.

## 2.4 WINSOC removal

WINSOC was removed from the water-extracted filters using a thermal–optical OC/EC analyser (Model 5L, Sunset Laboratory Inc., USA) for separation of EC. WINSOC removal was performed with the first three steps of the Swiss\_4S protocol, thus denoted Swiss\_3S. This allows for individual WINSOC removal runs and pooling of several filters for  $^{14}\text{C}(\text{EC})$  analysis. The water-extracted filters were cut in quadrants ( $0.64\text{ cm}^2$  each) to fit the OC/EC analyser sample holder ( $10 \times 15\text{ mm}$ ). Up to 12 WINSOC removal runs per single sample and 24 runs for pooled samples were performed. After WINSOC removal, the filters were stored in a freezer ( $-20^\circ\text{C}$ ) until  $^{14}\text{C}(\text{EC})$  analysis. In the final step, EC was combusted in the thermal–optical OC/EC analyser subjected to online radiocarbon measurement (Agrios et al., 2015). The protocol was modified to compensate for EC losses (see Sect. 2.10) observed with the standard protocol (Zhang et al., 2012). WINSOC removal was performed in these three steps: step 1 (pure  $\text{O}_2$ ,  $375^\circ\text{C}$ , 240 s), step 2 (pure  $\text{O}_2$ ,  $425^\circ\text{C}$ , 120 s), and step 3 (pure He,  $600^\circ\text{C}$ , 120 s). This procedure provided EC yields  $> 0.7$ .

## 2.5 Direct $^{14}\text{C}(\text{WSOC})$ measurement

Inorganic carbonaceous impurities were removed by acidification and helium flushing. For this,  $\text{H}_3\text{PO}_4$  (0.5 mL 8.5 %) freshly prepared from  $\text{H}_3\text{PO}_4$  (85 %, Suprapur grade, Merck KGaA, Germany) was added using a 1 mL Hamilton (Reno, NV, USA) glass syringe, and high-purity (99.999 %) helium was purged ( $50\text{ mL min}^{-1}$ ) through the sample at room temperature for 3 min. The sample septum was pierced with a

custom-made needle with a gas inlet and outlet hole, where the gas outlet was submerged ( $\sim 1\text{ cm}$ ) and the gas inlet was placed in the upper part of the headspace. These steps were robotically performed by a PAL HTC-xt (CTC Analytics AG, Switzerland) mounted on top of a carbonate handling system (CHS, Ionplus AG, Switzerland).

The chemical-wet-oxidation procedure was used to oxidise WSOC to  $\text{CO}_2$  for radiocarbon measurement (Lang et al., 2012; Wiedemeier et al., 2016). The oxidiser (10 % potassium persulfate; ACS grade, Sigma-Aldrich, USA) was freshly prepared, dissolved in  $\text{H}_3\text{PO}_4$  (5 %,  $\text{m m}^{-1}$ ), pre-oxidised ( $90^\circ\text{C}$ , 30 min), and flushed with helium ( $50\text{ mL min}^{-1}$ , 3 min) to remove all carbonaceous contaminants. Oxidiser (0.25 mL) was added to each sample, and the reaction progressed overnight at  $75^\circ\text{C}$  on the hot plate of the CHS. For sampling the generated  $\text{CO}_2$  ( $50\text{ mL min}^{-1}$ , 3 min), we used the custom-made needle and PAL autosampler described above. The CHS was connected to a custom-built water trap to retain liquid water in a wash bottle (25 mL), whereas the remaining water vapour was trapped using  $\text{P}_2\text{O}_5$  (SICAPENT<sup>®</sup>, Merck KGaA, Germany). The dry gas was then carried to the gas interface system (GIS) and trapped on a X13-zeolite trap (Ruff et al., 2007; Wacker et al., 2013). After sampling, the trapped  $\text{CO}_2$  was thermally released and mixed with helium for  $^{14}\text{C}$  measurement. The cross-contamination was determined in an earlier study (Agrios et al., 2015): after analysing fossil and modern samples alternately, 0.5 % of the carbon of the previous sample was found to mix and cross-contaminate the next injection. Therefore, we applied a cross-contamination of 0.5 % and a constant contamination of  $0.9 \pm 0.2\text{ }\mu\text{g C}$  with  $F^{14}\text{C} = 0.20 \pm 0.08$  on samples subjected to chemical wet oxidation (see Sect. S5 in the Supplement).

## 2.6 Online $^{14}\text{C}(\text{TC})$ and $^{14}\text{C}(\text{EC})$ measurement

A total of  $5.2\text{ cm}^2$  of each filter ( $16.6\text{ cm}^2$ ) was used for  $^{14}\text{C}(\text{TC})$  analysis and  $10.4\text{ cm}^2$  for pooled samples. The

$^{14}\text{C}(\text{TC})$  was measured by complete combustion (240 s, 870 °C, pure  $\text{O}_2$ ) in the Sunset OC/EC analyser before  $^{14}\text{C}$  analysis (see Sect. 2.7). Complete combustion was ensured by passing the evolved sample through the second furnace of the analyser containing  $\text{MnO}_2$  at 870 °C. The evolved  $\text{CO}_2$  was analysed by the non-dispersive infrared (NDIR) detector, resulting in 20.2–116.2 and 27.0–99.3  $\mu\text{g C}$  for single and pooled filters, respectively. An equivalent area was used for back filters, yielding 3.4–11.3 and 6.2–11.8  $\mu\text{g C}$  for single and pooled filters, respectively.

For  $^{14}\text{C}(\text{EC})$  analysis, the filters consisting of only EC after water extraction (see Sect. 2.3) and WINSOC removal (see Sect. 2.4) were combusted in the Sunset OC/EC analyser. Between 3.8 and 15.3  $\text{cm}^2$  of filter material was combusted for EC, yielding 3.9–16.8  $\mu\text{g C}$ . After combustion, the released gas was dried ( $\text{P}_2\text{O}_5$ , SICAPENT<sup>®</sup>, Merck KGaA, Germany) and transferred to the GIS where  $\text{CO}_2$  was trapped and thermally released for online measurement in the AMS (Agrios et al., 2015) (see Sect. 2.7). We applied a cross-contamination correction of 0.2 % due to a  $\text{CO}_2$  adsorption memory effect on the zeolite trap for TC and EC (Salazar et al., 2015). A constant-contamination correction of  $0.40 \pm 0.20 \mu\text{g}$  with  $F^{14}\text{C} = 0.80 \pm 0.36$  was applied. To account for EC loss and charring during TOA,  $F^{14}\text{C}(\text{EC})$  values were corrected using the “COMPYCALC” (COMprehensive Yield CALCulation) script (see Sect. 2.10).

## 2.7 Radiocarbon measurement

Radiocarbon measurement was performed using a MICADAS (Mini Carbon Dating System) accelerator mass spectrometer (AMS) at the University of Bern (Synal et al., 2007; Szidat et al., 2014; Fahrni et al., 2013). On each AMS measurement day, multiple OxII (oxalic acid ii, SRM 4990C, National Institute of Standards and Technology, NIST, Gaithersburg, MD, USA) and fossil NaAc (sodium acetate, Sigma-Aldrich, no. 71180) (Szidat et al., 2014) standards were analysed. BATS software version 3.6 (Wacker et al., 2010) was used for standard normalisation as well as for data correction for background, blank, and mass fractionation.

## 2.8 Contamination precautions

All filter handling and water extraction were performed in a laminar flow cabinet. All glassware was cleaned using  $\text{H}_3\text{PO}_4$  (1 M, ACS grade, Merck KGaA, Germany) and pre-fired (500 °C, 5 h), as described by Lang et al. (2012). The vials were leak-tested overnight at 75 °C and with  $\sim 4$  bar of  $\text{N}_2$ . The glass syringe used for water extraction was rinsed before use using ultrapure water and then pre-fired (500 °C, 2 h). The filter holders and silicone O-rings were rinsed and sonicated with ultrapure water before use and dried in a laminar flow cabinet.

## 2.9 EC correction model

OC/EC separation leads to losses of EC during thermal desorption, which need to be corrected by an  $F^{14}\text{C}(\text{EC})$  yield extrapolation. The correction supposes that the EC fraction consists of two subfractions, a subfraction with certain volatility at the temperature of steps S1, S2, and S3 and a refractory subfraction. The yield ( $Y$ ) and  $F^{14}\text{C}$  of EC ( $F_{\text{EC}}$ ) of the mixture are empirically determined as explained in Sect. 2.10 and 2.6, respectively. For further information,  $Y$  and  $F_{\text{EC}}$  are modelled from the mass balance as follows:

$$Y = \frac{m_v + m_{nv}}{m_{v0} + m_{nv0}} = \frac{q_m \times \alpha_v + \alpha_{nv}}{q_m + 1}, \quad (1)$$

$$\begin{aligned} F_{\text{EC}} &= \frac{m_v \times F_v + m_{nv} \times F_{nv}}{m_v + m_{nv}} \\ &= \frac{q_m \times \alpha_v \times F_v + \alpha_{nv} \times F_{nv}}{q_m \times \alpha_v + \alpha_{nv}}, \end{aligned} \quad (2)$$

$$q_m = \frac{m_{v0}}{m_{nv0}}. \quad (3)$$

The parameter  $q_m$  is the quotient of the initial masses of the non-refractory ( $m_{v0}$ ) to refractory ( $m_{nv0}$ ) subfractions, and it is calculated with Eq. (3).  $F_v$  and  $F_{nv}$  are the fraction modern of the non-refractory ( $F^{14}\text{C} = 1$ ) and refractory ( $F^{14}\text{C} = 0$ ) subfractions.  $\alpha_v$  is the mass fraction of the non-refractory EC subfraction that withstands the WINSOC removal procedure relative to the initial mass calculated as  $\alpha_v = m_v m_{v0}^{-1}$ .  $\alpha_{nv}$  is the analogue of  $\alpha_v$  for the refractory subfraction. Each step of the WINSOC removal has a value of  $\alpha$ , which is calculated with Eq. (4) by a first-order kinetic equation:

$$\alpha = e^{-t \times K(T)} = e^{-t \times K(T_{\text{ref}})} e^{\left(\frac{E_a}{RT_{\text{ref}}} - \frac{b \times E_a}{RT}\right)}, \quad (4)$$

where  $t$  is the step desorption time (s) and the desorption rate  $K$  ( $\text{s}^{-1}$ ) is calculated with the temperature-dependent Arrhenius equation. The global  $\alpha$  is the joint yield of all the steps  $\alpha = \alpha_1 \times \alpha_2 \times \alpha_3$ . Bedjanian et al. (2010) also used a first-order kinetic coupled to Arrhenius for investigating the thermal desorption of polyaromatic hydrocarbons (PAHs) from soot surfaces. The main composition of the EC fraction is soot with compounds molecularly similar to PAHs of diverse sizes. Bedjanian et al. (2010) found that the activation energy ( $E_a$ ) for PAHs is in the range of 85 to 134  $\text{kJ mol}^{-1}$ , linearly depending on the molecular weight for the range of 178–302  $\text{g mol}^{-1}$ . The desorption rate  $K$  was ranging from  $3 \times 10^{-3}$  to  $5 \times 10^{-5} \text{ s}^{-1}$  for a temperature range of 370–350 K. The Arrhenius pre-exponential factor was solved by using the concept of the reference temperature (Peleg et al., 2012; Schwaab and Pinto, 2007). The scale of the desorption rate  $K$  is logarithmic, meaning that a small increase or decrease in temperature leads to a substantial change in the

desorption rate. Our optimised  $E_a$  is  $100\text{ kJ mol}^{-1}$ , and our reference desorption rate  $K$  is  $1.5 \times 10^{-6}\text{ s}^{-1}$  at  $340\text{ K}$  ( $T_{\text{ref}}$ ), which is in the range of the desorption rates from Ghosh et al. (2001) converted from room temperature to our reference temperature. The information can be found in Table 3 of Ghosh et al. (2001) with values between  $1.2 \times 10^{-9}$  and  $3.6 \times 10^{-9}\text{ s}^{-1}$  at  $293\text{ K}$  ( $E_a = 116$  to  $133\text{ kJ mol}^{-1}$ ), which results in desorption rates at  $T_{\text{ref}} = 340\text{ K}$  of  $9 \times 10^{-7}$  to  $7 \times 10^{-6}\text{ s}^{-1}$ . The activation energy for the refractory fraction is unknown, but we may assume that the molecular weights of the compounds of the refractory fraction are much heavier. Bedjanian et al. (2010) showed a linear relationship between molecular size and volatility with  $E_a$ ; therefore, we introduce an empirical factor  $b$ , which represents how much bigger  $E_a$  is for the refractory relative to the non-refractory fraction as shown in Eq. (5).  $E_a$  and  $K(T_{\text{ref}})$  values were kept within the references ranges and optimised with the data from our previous works (see Sect. 3.1 and Fig. S2 in Zotter et al., 2014);  $E_a$  and  $K(T_{\text{ref}})$  were taken from the references;  $t$  and  $T$  were fixed to the WINSOC removal conditions.

$$E_{a_{\text{nv}}} = b \times E_{a_v} \quad (5)$$

The values for the parameters  $b$  and  $q_m$  are optimised for each individual sample as follows. The  $q_m$  and  $b$  parameters are selected; the mathematical model estimates  $\alpha$  for both refractory and non-refractory fractions with Eqs. (4) and (5). Then the yield and  $F_{\text{EC}}$  are calculated with Eqs. (1) and (2). The yield and  $F_{\text{EC}}$  from the model are compared with the empirical yield and  $F_{\text{EC}}$  using a cost function shown in Eq. (6). The cost function is minimised by a gradient descent method from the R script.  $q_m$  and  $b$  are not general parameters or general coefficients; usually their values are different between samples because their molecular compositions are different. The number of data values in the cost function is only two.

$$J(q_m, b) = [F_{\text{EC, data}} - F_{\text{EC, model}}(q_m, b)]^2 + [Y_{\text{data}} - Y_{\text{model}}(q_m, b)]^2 \quad (6)$$

Our model is a two-component model used to describe a multicomponent system. Two-component models are common: for example, the Keeling approach to describe the mixing of one component onto a background component in complex atmospheric air or dissolved organic carbon in ocean waters (Keeling, 1958; Walker et al., 2016). Each refractory and non-refractory subfraction is composed of a complex mixture of compounds with a continuum of volatilities and  $^{14}\text{C}$  content. However, the mean desorption energy of the subfractions obeys Eq. (5). The  $^{14}\text{C}$  content of both subfractions is not exactly 1.0 or 0.0 but a continuum where the mean  $F^{14}\text{C}$  of the refractory subfraction tends towards fossil values, while the opposite occurs to the non-refractory subfraction.

## 2.10 EC and OC correction calculations

The  $F^{14}\text{C}(\text{EC})$  yield extrapolation and charring correction were performed with a script named COMPYCALC (Comprehensive Yield CALCulation, version 1.3.0) written in R (R Core Team, 2020), available on GitHub (<https://github.com/martin-rauber/compycalc>, last access: 27 January 2023) and archived in Zenodo (Rauber and Salazar, 2022). Using Eq. (7), an initial value of  $F^{14}\text{C}(\text{OC})$  is calculated prior to running the script using the uncorrected  $F^{14}\text{C}(\text{EC})$  value, as  $F^{14}\text{C}(\text{OC})$  is needed for the charring correction (see Table S1 in the Supplement).  $F_{\text{TC}}$  and  $F_{\text{EC}}$  are the radiocarbon values (fraction modern,  $F^{14}\text{C}$ ) for TC and EC before correction, respectively, whereas  $r$  is the EC/TC ratio.

$$F_{\text{OC}} = \frac{F_{\text{TC}} - F_{\text{EC}} \times r}{1 - r} \quad (7)$$

The EC yield was calculated using the laser transmission signal (655–660 nm) of the OC/EC analyser. Each WINSOC raw data file from the Sunset OC/EC analyser is loaded by the COMPYCALC script. The laser transmission is dependent on the temperature (Peterson and Richards, 2002). By applying a correction to the complete laser signal of the thermogram, this temperature-induced change in transmission is accounted for. For COMPYCALC, a generic file corresponding to the S4 step in the Swiss\_4S protocol is used for the calculation of the temperature dependence correction of the laser transmission signal. The EC yield ( $Y$ ) after the three WINSOC removal steps was calculated as the ratio of the attenuation (ATN) after S3 to the initial ATN after water extraction. ATN is a unitless parameter proportional to the light-absorbing EC mass calculated using the Beer–Lambert law and the laser transmission signal (Gundel et al., 1984; Zhang et al., 2012). Here, the temperature dependence correction of the laser transmission signal is applied. Formation of pyrolysed OC (i.e. charring; see below) is quantified by the ratio of the difference between the maximum ATN and the initial ATN of each step (Gundel et al., 1984; Zhang et al., 2012; Vlachou et al., 2018). When filter punches do not cover the sample holder spoon area completely, small filter movements from vibrations caused by the OC/EC analyser may occur. This may inflict faulty laser signals when filters are smaller than the sample holder area ( $10 \times 15\text{ mm}$ ). WINSOC removal is usually performed on multiple filter cuts, and EC yield and charring are calculated for each filter cut. COMPYCALC filters by the interquartile range of  $< 1.5$  individually for EC yield and charring in S1, S2, and S3 and removes the row(s) containing outliers in the data frame. The number of filters cuts used for calculation is summarised in Table S5. The COMPYCALC summary output (see Fig. S2 and Table S2 in the Supplement) only includes the filtered data; however, the raw data (not filtered) are preserved and given as an output as well. The EC yield and charring before filtering are shown in Table S6.

The measured  $F^{14}\text{C}(\text{EC})$  values ( $F_{\text{EC}}$ ) were extrapolated to 100 % EC yield ( $F_{\text{EC}(\text{corr})}$ ) using Eq. (9) to account for the EC loss during WINSOC removal. For the empirical data, the yield  $Y$  and the  $F_{\text{EC}}$  are directly measured, while  $\alpha$  is calculated with Eq. (4). The reader must note that Eq. (8) is obtained when Eq. (1) is input in the denominator of Eq. (2) and solving for parameter  $q_m$ . If  $Y = 1$ , then Eq. (8) becomes the  $F_{\text{EC}}$  extrapolated at 100 % yield (Eq. 9).

$$F_{\text{EC}} = \frac{q_m \times \alpha_v \times F_v + \alpha_{\text{nv}} \times F_{\text{nv}}}{Y(1 + q_m)} \quad (8)$$

$$F_{\text{EC}(\text{corr})} = \frac{q_m \times F_v + F_{\text{nv}}}{1 + q_m} \quad (9)$$

Besides extrapolation to 100 % EC yield, the fraction modern must be corrected for charring as some OC is pyrolysed into EC. Pyrolytic carbon (PC) was quantified using the ATN signal for each step. We typically observed an ATN increase caused by PC formation at the moment when the temperature was increased, whereas the onset of ATN decrease due to EC losses occurred later in each step so that both processes were detected separately. However, we cannot exclude the possibility that PC formation that may have developed later in the temperature steps was masked by large EC losses. Nevertheless, we regard this as negligible, as the fractions of charring were anyway rather small. The charring-corrected fraction modern ( $F_{\text{charrA}}$ ) is calculated in Eq. (10) using the fraction modern of EC ( $F_{\text{EC}(\text{corr})}$ ) extrapolated to 100 %. The fraction modern of OC ( $F_{\text{OC}}$ ) was previously calculated using Eq. (7);  $\varepsilon$  is the total charring. It is assumed that 50 % of the pyrolysed OC (i.e. pyrolytic carbon, PC) is lost in the subsequent temperature steps again, adding to the observed EC loss (Zotter et al., 2014). Furthermore, Chow et al. (2004) reported that the mass absorption coefficient (MAC) of PC may be 2.5 times larger than the MAC of EC, which is also consistent with Boparai et al. (2008). We therefore considered that the actual PC concentration is only 40 % of its apparent value from ATN determination according to the approach of Winiger et al. (2015). Consequently, a factor of 0.2 is used to correct for both the losses of PC during the thermal treatment and the effect of the different MAC values of PC and EC. For Eq. (11), the fraction modern of EC without extrapolation to 100 % EC yield is used. In Eq. (12), the fraction modern with charring correction ( $F_{\text{charrC}}$ ) is calculated with the charring correction slope  $\beta$  and EC yield ( $Y$ ).  $\beta$  is the slope between the fraction modern and EC yield as defined previously (Zotter et al., 2014; Zhang et al., 2012). The final fraction modern with charring correction in Eq. (13) is calculated as the mean of Eqs. (10) and (12).

$$F_{\text{charrA}} = \frac{F_{\text{EC}(\text{corr})} - F_{\text{OC}} \times 0.2 \times \varepsilon}{1 - 0.2 \times \varepsilon} \quad (10)$$

$$F_{\text{charrB}} = \frac{F_{\text{EC}} - F_{\text{OC}} \times 0.2 \times \varepsilon}{1 - 0.2 \times \varepsilon} \quad (11)$$

$$F_{\text{charrC}} = \beta \times (1 - Y) + F_{\text{charrB}} \quad (12)$$

$$F_{\text{EC}(\text{final})} = \frac{F_{\text{charrA}} + F_{\text{charrC}}}{2} \quad (13)$$

After all calculations, a data file with overall EC yield, the charring contribution for each OC removal step (S1, S2, S3), and the total charring contribution as well as the  $F^{14}\text{C}(\text{EC})$  input value  $F_{\text{EC}}$ ,  $F^{14}\text{C}(\text{EC})$  extrapolated to 100 % EC yield ( $F_{\text{EC}(\text{corr})}$ ), and  $F^{14}\text{C}(\text{EC})$  extrapolated to 100 % EC yield and corrected for charring ( $F_{\text{EC}(\text{final})}$ ) is generated as an output. The final  $F^{14}\text{C}(\text{OC})$  is calculated using Eq. (7) with  $F_{\text{EC}(\text{corr})}$  and is reported as  $F_{\text{OC}(\text{corr})}$ . Estimated uncertainties in  $F_{\text{EC}(\text{final})}$  and  $F_{\text{OC}(\text{final})}$  amount to  $\pm 15\%$  and  $\pm 4\%$ , respectively.

## 2.11 EC yield calculation and WINSOC amount calculation

EC yield calculation and amount calculation of each WINSOC step were performed with the R script “Sunset-calc”, written as an R Shiny application (R Core Team, 2020; Chang et al., 2017). Sunset-calc provides amount calculation for each step in the Swiss\_3S and Swiss\_4S protocols (Zhang et al., 2012) as well as EC yield and charring calculation (see Table S7). Furthermore, EC yield and charring-corrected OC (WINSOC) and EC amounts are calculated (see Table S4). The Sunset OC/EC analyser raw files are loaded in a web graphical user interface, and the results are received as a downloadable file. EC yield and charring calculation is based on COMPHYCALC as described in Sect. 2.9. The amount calculation is made with an integration of the NDIR signal. The application has been deployed on an R server (<http://14c.unibe.ch/sunsetcalc>, last access: 27 January 2023). Sunset-calc is available on GitHub (<https://github.com/martin-rauber/sunset-calc>, last access: 27 January 2023) and archived in Zenodo (Rauber, 2021).

## 3 Results and discussion

### 3.1 Validation of the correction

Figure 2a shows the comparison of the modelled  $F_{\text{EC}}$  vs. the empirical  $F_{\text{EC}}$ , and Fig. 2b shows the modelled EC yield vs. the empirical EC yield. The empirical data are taken from Fig. S2 of our previous work (Zotter et al., 2014). Figure 2a and b indicate that our model provides good accuracy for predicting the  $F_{\text{EC}}$  and the EC yields. We determined a relative accuracy of  $109 \pm 4\%$  as an agreement of the measured values compared to the modelled values using a linear model and its residual standard uncertainty. Therefore, the  $b$  and  $q_m$  values are reliable. Figure 2c indicates that the  $b$  parameter



falls into two volatility groups: the group close to  $b = 1.0$  and the group mainly within 2.0 to 2.5. These are interesting results as the initial value for  $b$  is 2.0 at the start of the gradient descent optimisation. We examined the optimisation again, and the script does check values in the range of 1.0 to 2.0. Figure 2c is an indirect probing of the volatility of the sample compounds. Figure 2d shows the calculated parameters for each sample, revealing that  $q_m$  increases with  $F_{\text{EC}}$ . This indicates that for higher  $F_{\text{EC}}$  values, closer to the atmospheric non-fossil levels, the initial mass of the non-refractory biogenic EC (Sect. 2.9) subfraction must be higher than the initial mass of the refractory EC subfraction with the higher fossil proportion.

Figure 2e provides examples of the modelling of the  $F_{\text{EC}}$  vs. the modelled EC yields for different values of the parameter  $b$ . The EC yield is decreased by proportionally increasing the temperature of each of the three steps of the WINSOC removal. The model allows us to extrapolate the  $F_{\text{EC}}$  value of any sample with a yield lower than 100 % to the  $F_{\text{EC}}$  value corresponding to 100 % yield, which defines the correction for EC loss. According to the Arrhenius approach, the model has a non-linear shape which may be approximated by a linear model in the region of EC yields higher than 0.5. Before developing this non-linear model, we applied a simple linear model for the EC loss correction according to previous publications (Zotter et al., 2014). The measurement conditions usually keep the EC yield higher than 0.4; thus the linear model remains useful under certain conditions. Nevertheless, the non-linear model is superior and shall be used in future. Figure 2f is similar to Fig. 2e but for different  $q_m$  values. As shown in Zotter et al. (2014), different samples may show different slopes and intercepts for the linear model. Figure 2e and f show that different values of  $b$  and  $q_m$  explain the different slopes and intercepts observed previously in the data. Extrapolation and correction to  $F_{\text{EC}(\text{corr})}$  of the data from Zotter et al. (2014) are shown in Fig. S6. In Fig. S6, same-colour results belong to punches from the same filter; however the experimental conditions of their online  $^{14}\text{C}(\text{TC})/^{14}\text{C}(\text{EC})$  measurements were varied in order to obtain different yields and  $F_{\text{EC}}$  values. Therefore, the same-colour results in Fig. S6, ideally, should have the same  $F_{\text{EC}}$  value extrapolated to 100 % yield. As indicated in Sect. 2.9, these data were useful to optimise the  $E_a$  and  $K(T_{\text{ref}})$  values by minimising the differences between the yield-corrected  $F_{\text{EC}}$  of the same-colour results. This optimisation was performed prior to the application of the non-linear model to the results of this paper.

For validation of the correction method for  $^{14}\text{C}(\text{EC})$  presented here, the use of reference material could offer a means. Reference materials were not measured, however, as most of those that are provided are in powder form only (Baumgardner et al., 2012). This powder must be dispersed homogeneously on a filter first, which is difficult to achieve and usually leads to inhomogeneities, which even worsens if water extraction is employed on this dispersed powder. Fur-

thermore, such reference materials (e.g. NIST SRM 1649a) typically contain a certain fraction of coarse particles of up to  $100\text{ }\mu\text{m}$ , which is substantially larger than the  $\text{PM}_{10}$  size cut from the field samples. According to our experience, coarse particles differ in the OC/EC separation and charring behaviour from field samples collected with a  $\text{PM}_{10}$  size cut or smaller. To our knowledge, only one reference material exists that is provided on quartz fibre filters, which is NIST SRM 8785 (i.e. SRM 1649a dispersed on filter material using a  $\text{PM}_{2.5}$  size cut). However, the intercomparison study of Szidat et al. (2013) with this reference material showed inhomogeneities that were caused in the dispersion process. Due to this situation, method validation may still be more effective today if based on thoroughly analysed and well-homogenised high-volume filters. Additionally, employing or omitting water extraction is crucial for an agreement between individual labs even when applying different EC isolation techniques. Most participants in the aerosol intercomparison study from Szidat et al. (2013) did not employ water extraction, which resulted in a larger scatter compared to Zenker et al. (2017), where all participants used water extraction to reduce charring. Nevertheless, as no suitable reference material exists, the validation of this method is currently not possible, and therefore it cannot be considered fully validated.

### 3.2 Concentrations of carbonaceous aerosols

Results from the 21-month sampling period (Table 1) showed a mean TC concentration of  $137\text{ ng C m}^{-3}$  (range:  $65\text{--}264\text{ ng C m}^{-3}$ ) and a mean EC concentration of  $14\text{ ng C m}^{-3}$  (range:  $3\text{--}40\text{ ng C m}^{-3}$ ), resulting in a mean OC/EC ratio of 11.7 (range:  $4.5\text{--}27$ ). The filters sampled from 28 September to 6 October 2017 had elevated TC ( $601\text{ ng m}^{-3}$ ) and EC ( $52\text{ ng C m}^{-3}$ ) levels and were excluded from the mean reported above as this would clearly distort the mean. The OC/EC ratio for this filter sample was 10.5 and thus comparable to the mean of the other samples. For 5 of the 13 samples, 2 consecutive filter samples were pooled to obtain a sufficient carbon amount for  $^{14}\text{C}$  analysis (see Table 1). Lower TC values were seen in winter (November to March) compared to summer (April to October), whereas it was the other way around for EC. Consequently, the OC/EC ratio shows a seasonality with lower values in winter and higher values in summer. TC on back filters had a mean concentration of  $22\text{ ng C m}^{-3}$  (range:  $12\text{--}49\text{ ng C m}^{-3}$ ) and showed no seasonality. The mean pure WINSOC concentration (Table 2), corresponding to step 1 of the Swiss\_3S protocol, was  $26\text{ ng C m}^{-3}$  (range:  $9\text{--}71\text{ ng C m}^{-3}$ ), whereas the mixed (WINSOC + EC) S2 and S3 fractions had mean concentrations of  $4\text{ ng C m}^{-3}$  (range:  $0.5\text{--}26\text{ ng C m}^{-3}$ ) and  $7\text{ ng C m}^{-3}$  (range:  $1.5\text{--}16\text{ ng C m}^{-3}$ ). The aforementioned high-loading filter sample values from the transition September–October 2017 ( $111\text{ ng C m}^{-3}$ , S1;  $26\text{ ng C m}^{-3}$ , S2; and  $27\text{ ng C m}^{-3}$ , S3) were excluded from the mean. The total amount of WINSOC including EC loss was  $37\text{ ng C m}^{-3}$  (range:  $1.5\text{--}$



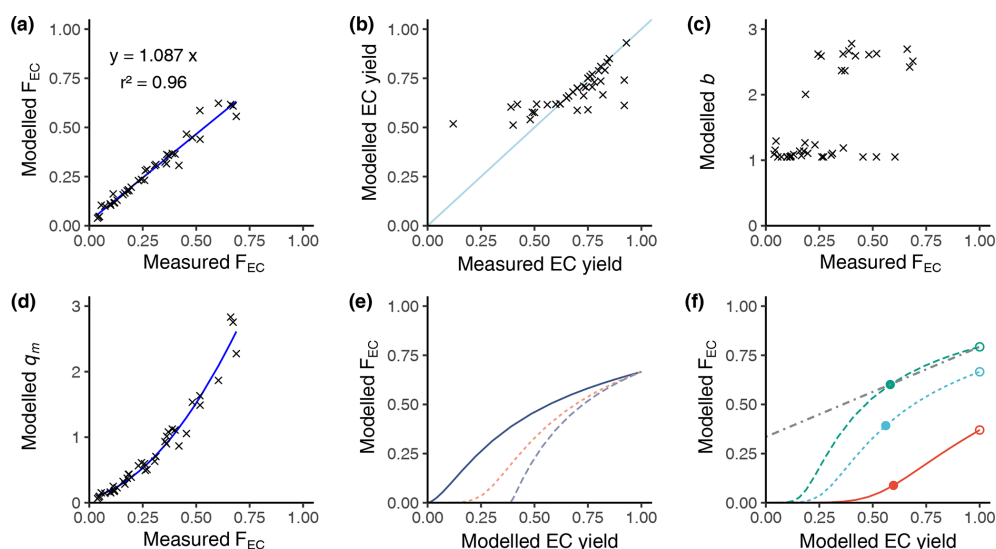


**Figure 2.** Summary of the modelled EC correction to an EC yield of 1. (a) Model accuracy: modelled  $F_{\text{EC}}$  vs. measured  $F_{\text{EC}}$ . (b) Modelled EC yield vs. measured EC yield according to Zotter et al. (2014) (see text). (c) Model calculated parameters  $b$ . (d) Model calculated parameters  $q_m$ . (e) General behaviour of  $F_{\text{EC}}$  vs. EC yield for different  $b$  values (solid line  $b = 1.1$ , dashed orange line  $b = 1.2$ , long blue line  $b = 1.5$ ) with a fixed  $q_m$  of 1.5. (f) General behaviour of  $F_{\text{EC}}$  vs. EC yield for different  $q_m$  values (solid line  $q_m = 0.5$ , dashed green line  $q_m = 1.5$ , dashed cyan line  $q_m = 2.5$ ) with a fixed  $b$  value of 1.2 and a linear model (dash-dotted line) for a sample with extrapolation at an EC yield of 1. Filled dots show the measured value, and the open dots show the value after extrapolation.

$16 \text{ ng C m}^{-3}$ ; excluded filter:  $164 \text{ ng C m}^{-3}$ ). WSOC was calculated by subtracting EC and total WINSOC from TC, which gave a mean of  $39 \text{ ng C m}^{-3}$  (range:  $0.5\text{--}92 \text{ ng C m}^{-3}$ ). The September–October 2017 filter sample had a loading of  $284 \text{ ng C m}^{-3}$  and was excluded from the mean. The mean amount corrected for charring and EC loss calculated with Sunset-calc (see Sect. 2.11, Table S4) for WINSOC was  $34 \text{ ng C m}^{-3}$  (range:  $11\text{--}90 \text{ ng C m}^{-3}$ ; excluded filter:  $151 \text{ ng C m}^{-3}$ ), and the mean amount corrected for EC was  $15 \text{ ng C m}^{-3}$  (range:  $3.7\text{--}39 \text{ ng C m}^{-3}$ ; excluded filter:  $67 \text{ ng C m}^{-3}$ ). For these calculations and corrections, the R Shiny application Sunset-calc was necessary as they were not possible with the default software tools provided for the Sunset OC/EC analyser. The  $^{14}\text{C}(\text{TC})$  measurements on back filters (see Table 3) revealed a mean filter loading of  $90 \text{ ng C m}^{-3}$  (range:  $26\text{--}189 \text{ ng C m}^{-3}$ ) excluding the autumn 2017 filter, which had a back filter loading of  $501 \text{ ng C m}^{-3}$ .

### 3.3 Development of preparation methods

#### 3.3.1 Water extraction

For water extraction, three filter punches were stacked to maximise the amount of extractable WSOC. Prior to filter sample extraction, trials with empty filters and the screw type polycarbonate water extraction unit were made. Stacking more than three filters was not feasible, as it makes the water extraction housing prone to leakage. The sample water extraction was gravity-fed. Ultrapure water was filled in the

pre-combusted glass syringe directly from the tap of the ultrapure water system and screwed onto the previously assembled water extraction unit to avoid unnecessary liquid transfer. The extraction of 5 mL took 2–3 min depending on the number of filters stacked.

The water-extracted filter material was subjected to WINSOC removal and  $^{14}\text{C}(\text{EC})$  measurement. Elimination of WSOC is beneficial as it is shown to pyrolyse into EC (charring) when subjected to thermal–optical analysis (Yu et al., 2002; Cadle et al., 1980). The  $F^{14}\text{C}(\text{OC})$  is generally higher than for  $F^{14}\text{C}(\text{EC})$  (Szidat et al., 2004b, 2009; Zhang et al., 2012) but is often exceeded by  $F^{14}\text{C}(\text{WSOC})$  due to substantial contributions from biogenic sources and biomass-burning emissions (Zhang et al., 2014a; Kirillova et al., 2013; Weber et al., 2007). Therefore, a small contribution of charred OC significantly biases the measured  $F^{14}\text{C}$  of the EC fraction, which is prevented by the WSOC removal.

#### 3.3.2 Adaptations of the OC / EC analyser for WINSOC removal

The filter holders for water extraction are of screw type; thus round punches were required for water extraction. For WINSOC removal, a single layer of filter material cannot exceed the area ( $1.5 \text{ cm}^2$ ) of the sample holder spoon in the Sunset OC/EC analyser. Although it is not necessary to fully cover the sample holder area, the filter cut should cover most of the area to utilise the laser transmission signal for calculations. Stacking of filters should be avoided, as lower filters may not encounter the same conditions as the topmost filter,

**Table 1.** OC/EC ratios and filter loadings measured by NILU using the EUSAAR\_2 protocol. Filters that were pooled for  $^{14}\text{C}$  analysis are marked with an asterisk.

Start date	End date	TC ( $\text{ng C m}^{-3}$ )	EC ( $\text{ng C m}^{-3}$ )	OC ( $\text{ng C m}^{-3}$ )	OC/EC ratio
23 February 2017	2 March 2017	256	40	216	5.4
5 May 2017	15 May 2017	158	24	135	5.7
31 May 2017	26 June 2017	123	6	117	20.5
8 September 2017*	28 September 2017	114	6	108	16.7
28 September 2017	6 October 2017	601	52	549	10.5
6 October 2017*	24 October 2017	88	8	81	10.4
5 December 2017*	21 December 2017	73	12	61	7.7
23 January 2018	31 January 2018	174	16	157	9.6
21 March 2018	29 March 2018	127	18	109	6.1
6 April 2018	16 April 2018	129	17	111	6.4
12 July 2018*	30 July 2018	65	3	62	20.7
30 July 2018*	15 August 2018	264	9	254	27.0
23 November 2018	3 December 2018	72	13	59	4.5

\* Pooled filters.

**Table 2.** WINSOC amounts for each step of the Swiss\_3S protocol measured at the University of Bern and corresponding WSOC amounts. Fraction S1 is considered pure WINSOC, whereas S2 and S3 are mixed fractions of WINSOC and EC. WSOC was determined by subtraction of EC and total WINSOC from TC.

Start date	End date	WINSOC ( $\text{ng C m}^{-3}$ )				WSOC ( $\text{ng C m}^{-3}$ )	WSOC / WINSOC ratio
		S1	S2	S3	total		
23 February 2017	2 March 2017	43	10	16	70	92	1.6
5 May 2017	5 May 2017	20	3	8	31	70	2.5
31 May 2017	26 June 2017	71	9	12	93	4	< 0.1
8 September 2017*	28 September 2017	13	1	2	16	15	1.6
28 September 2017	6 October 2017	111	26	27	164	284	1.9
6 October 2017*	24 October 2017	9	1	2	12	15	1.7
5 December 2017*	21 December 2017	13	1	4	18	0	1.3
23 January 2018	31 January 2018	33	5	15	54	59	1.1
21 March 2018	29 March 2018	29	3	5	38	57	1.6
6 April 2018	16 April 2018	26	4	8	37	54	1.5
12 July 2018*	30 July 2018	11	0	1	13	7	0.7
30 July 2018*	15 August 2018	23	2	3	28	65	2.7
23 November 2018	3 December 2018	22	5	4	32	26	0.9

\* Pooled filters.

especially in terms of oxygen supply, which may cause differences with respect to both charring and EC losses within the stack. Furthermore, calculating an EC yield is not feasible after stacking two or more filters. We observed spikes in the laser transmission signal for small filter punches ( $< 0.5 \text{ cm}^2$ ), possibly due to filter movements caused by instrument vibrations. Due to the limitation of circular cuts for water extraction and a rectangular sample holder in the OC/EC analyser, the water-extracted filter was cut in quadrants. This enables the complete use of filter material; however, at the expense of a more labour-intensive WINSOC removal. The three water-extracted punches from each filter were cut into

12 and 24 quadrants for each individual and pooled sample, respectively. WINSOC was then removed from each sector using the Swiss\_3S protocol (Zhang et al., 2012), requiring 18.5 min per run. High EC losses were observed with the standard Swiss\_3S protocol; hence the protocol was adapted. Decreasing the temperature from 450 to 425 °C in S2 and from 650 to 600 °C in S3 increased EC yields from  $< 0.4$  to 0.6. Shortening the 600 °C pure He step in S3 from 180 to 120 s, further reduced EC losses, leading to a mean EC yield of 0.87 (range: 0.72–0.95) (Figs. 3 and 4). As shown in Fig. 4, the average charring after WINSOC removal was 2.8 % (range of 1 %–6.8 %) for S1, 0.6 % (0 %–2.4 %) for

**Table 3.** Filter loadings and fractions for front and back filters for TC measured at the University of Bern.

Start date	End date	TC front filter ( $\text{ng C m}^{-3}$ )	TC back filter ( $\text{ng C m}^{-3}$ )	$\text{TC}_P$ ( $\text{ng C m}^{-3}$ )
23 February 2017	2 March 2017	189	n.d.	n.d.
5 May 2017	15 May 2017	121	28	93
31 May 2017	26 June 2017	113	26	87
8 September 2017*	28 September 2017	39	11	29
28 September 2017	6 October 2017	501	49	453
6 October 2017*	24 October 2017	35	10	25
5 December 2017*	21 December 2017	36	9	27
23 January 2018	31 January 2018	135	14	121
21 March 2018	29 March 2018	109	15	94
6 April 2018	16 April 2018	105	35	70
12 July 2018*	30 July 2018	26	n.d.	n.d.
30 July 2018*	15 August 2018	104	n.d.	n.d.
23 November 2018	3 December 2018	67	12	54

\* Pooled filters. n.d.: not determined.

S2, and 3 % (1.3 %–9.0 %) for S3, with a total charring of 6.5 % (2.5 %–12.9 %). The OC and EC concentrations must be corrected for charring and EC losses using Sunset-calc (see Sects. 2.11 and 3.2). This enables a simple WINSOC removal protocol optimisation and adaptation after each run. The outcome of Sunset-calc is also employed for the correction of biases of  $^{14}\text{C}(\text{EC})$  results caused by charring and EC losses (see Sect. 3.4.1).

In the present work, WINSOC was removed but not subjected to radiocarbon measurement due to the very low filter loading. In the Swiss<sub>3</sub>S protocol, only the S1 fraction consists of pure WINSOC, as S2 and S3 are considered a mixture of WINSOC and EC. The average WINSOC loading in S1 was  $1.8 \mu\text{g C cm}^{-2}$ , ranging from 0.9 to  $3.7 \mu\text{g C cm}^{-2}$ , whereas radiocarbon measurements require at least  $3 \mu\text{g C}$ . With more highly loaded filters,  $^{14}\text{C}(\text{WINSOC})$  measurements can be implemented in the workflow presented.

### 3.3.3 Wet oxidation and WSOC measurement

Filter extraction and chemical wet oxidation may add contaminants, and stringent preparations (Sect. 2.5) were needed to ensure low procedural blanks. This included the use of acid-cleaned (high-purity-grade  $\text{H}_3\text{PO}_4$ ) and baked-out glassware and pre-oxidation of the oxidiser solution used to remove contaminants. The freshly prepared oxidiser solution was pre-oxidised at  $90^\circ\text{C}$  for 30 min before helium flushing with helium to remove carbonaceous contaminants. This step removes contaminants in the oxidiser itself as well as in the ultrapure water and equipment used. The oxidiser concentration was increased to 10 % from 4 %, whereas the amount of oxidiser added to the sample was reduced to 0.25 mL from 1 mL, compared to Lang et al. (2012). Oxidation was performed at  $75^\circ\text{C}$  overnight, deviating from previous studies by Lang et al. (2012) ( $100^\circ\text{C}$  for 60 min) and

Lang et al. (2013) ( $90^\circ\text{C}$  for 30 min). EXETAINER<sup>®</sup> vials store gas with little leakage even after multiple needle punctures (Glatzel and Well, 2008). All vials used for samples, standards, and blanks were leak-tested before use (Sect. 2.8) at the same temperature ( $75^\circ\text{C}$ ) as the oxidation step takes place. Vials are more prone to leakage at higher temperatures; hence we lowered the reaction temperature to  $75^\circ\text{C}$ . Both leak testing and a lower reaction temperature kept loss of precious sample material at a minimum. The sample acidification, helium flushing, and chemical wet oxidation were performed the day before measurement. The butyl rubber septum of the EXETAINER<sup>®</sup> may contaminate the sample over time when exposed to the strongly acidic and oxidative environment. As a cautionary principle, samples should be measured the day after preparation to minimise any losses, contaminations, and potential isotopic fractionation. In the present work, helium was purged at  $75^\circ\text{C}$  with the gas needle through the oxidised sample, unlike in Lang et al. (2012), where only the headspace was sampled at room temperature. Considerable amounts of liquid ( $\sim 0.3$  mL per sample) that were carried with the gas were trapped in a custom-built gas wash bottle (25 mL). Remaining water vapour was removed by a SICAPENT<sup>®</sup> trap ( $\text{P}_2\text{O}_5$  on inert carrier material) to protect the zeolite trap in the gas interface system (GIS). The  $\text{CO}_2$  amount was determined by the GIS pressure gauge based on the ideal gas law before dilution with helium and feeding the gas mixture into the ion source of the AMS. This procedure provides an estimation of the amount of WSOC only.

### 3.3.4 Procedural blank

The WSOC procedural blank was determined by performing the water extraction and wet-oxidation procedure, using pre-baked (2 h,  $750^\circ\text{C}$ ) quartz fibre filters (Pallflex<sup>®</sup> Tissuquartz

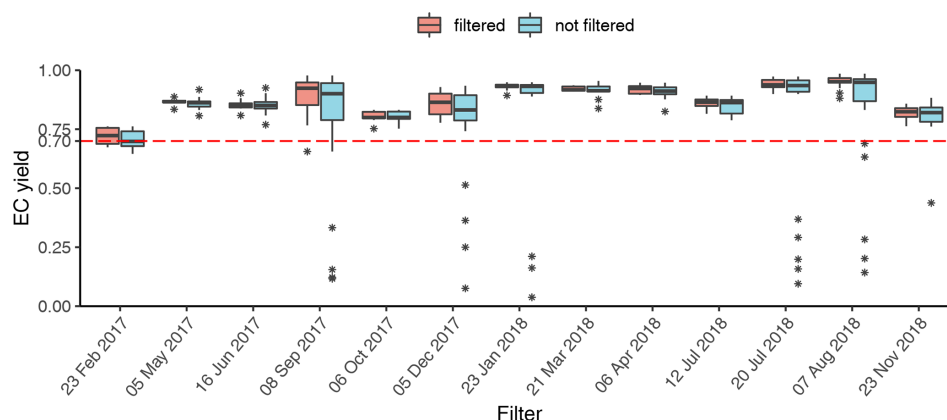


**Figure 3.** EC yield after WINSOC removal for each filter with the sampling start date. Filtered (WINSOC removal containing outliers in EC yield, fraction of charring S1, S2, or S3 removed) and unfiltered EC yields for each filter are shown. The boxplot box shows the first and third quartiles with the mean as a thick horizontal line for the individual groups (filtered and not filtered). The values outside the 1.5 interquartile range are shown with an asterisk. The horizontal line at 0.7 shows that at least 70 % of the initial EC has been recovered.

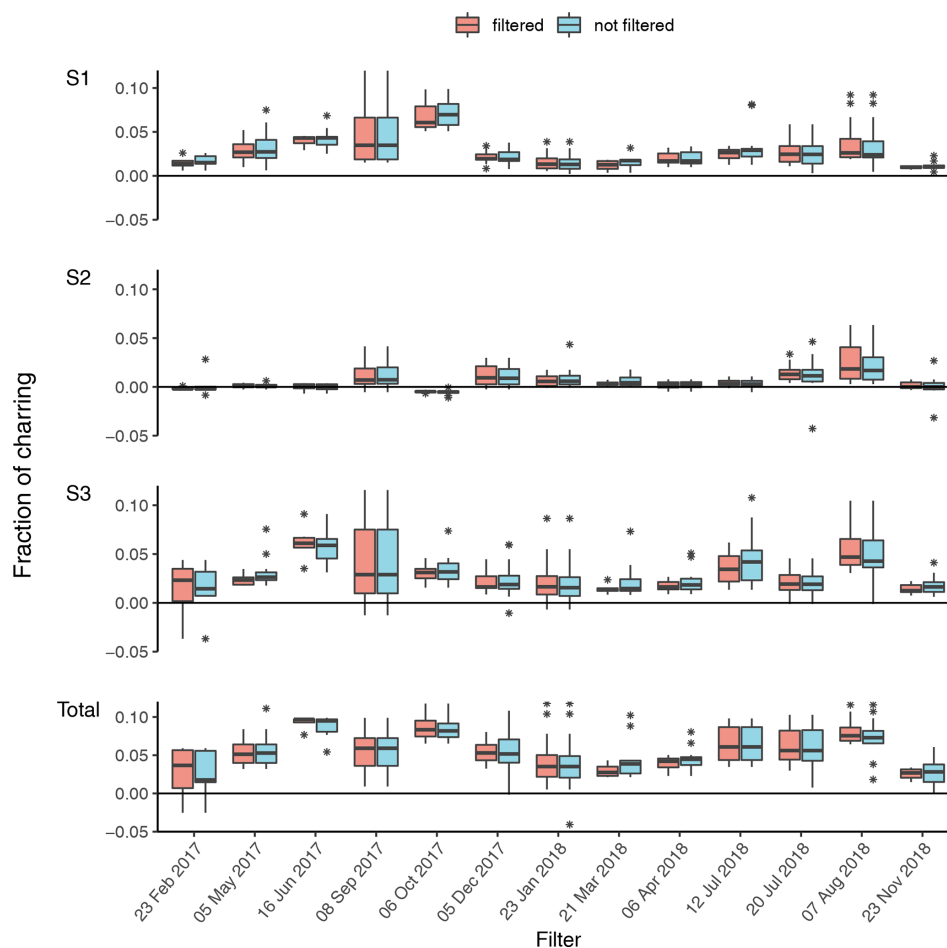


**Figure 4.** Fraction of charring observed for each filter at the individual steps (S1, S2, S3) and the total (sum of S1, S2, S3) with the sampling start date. Filtered (WINSOC removal containing outliers in EC yield, fraction of charring S1, S2, or S3 removed) and unfiltered fractions of charring for each filter are shown. The fraction of charring describes the amount of artificially produced EC by charring OC related to the amount of EC on the filter based on the laser transmission signal; i.e. a total charring of 0.05 means a 5 % contamination of the total EC amount.

2500QAT-UP), as described in Sect. 2.3. After extraction, different amounts of OxII (SRM 4990C) or fossil NaAc solutions ( $\sim 1000$  ppm) were added to the vials and subjected to chemical wet oxidation (Sect. 2.4). The mass and fraction modern of the contaminant were determined based on the constant-contamination approach by a drift model (Hanke et al., 2017; Salazar et al., 2015) (see Fig. S7). In previous studies, the WSOC eluate was dehydrated by lyophilisation before re-dissolving and combustion in an elemental analyser coupled to an AMS (Zhang et al., 2014a). Compared to the lyophilisation method, the procedural blank was lower for chemical wet oxidation, with a mass of contamination of  $0.9 \pm 0.2 \mu\text{g C}$  and the corresponding  $F^{14}\text{C}$  of  $0.20 \pm 0.08$ .

### 3.4 Radiocarbon results

#### 3.4.1 Correction of the $^{14}\text{C}(\text{EC})$ results

Early approaches of  $^{14}\text{C}(\text{EC})$  measurements focused on the separation of OC and EC (Zhang et al., 2012; Barrett et al., 2015; Zencak et al., 2007); however, some OC pyrolyses into EC, creating a positive artefact, and some EC is lost by desorption, degradation, or oxidation (Cadle et al., 1980; Yu et al., 2002; Gundel et al., 1984; Zhang et al., 2012), but efforts to correct  $^{14}\text{C}(\text{EC})$  were not considered then (Szidat et al., 2006, 2004b, a; Dusek et al., 2014; Andersson et al., 2011; Bernardoni et al., 2013). Zhang et al. (2012) implemented a linear correction for EC losses to account for the underestimation of biomass-burning EC. The composition of OC and EC underlies spatial and temporal variability, and thus the linear correction slope will differ. Zotter et al. (2014) addressed this issue by introducing different slopes for winter and summer, as the linear correction slope for EC differs considerably between these two seasons. Consequently, the linear correction slope must be either established for each site with multiple EC yield measurements or estimated based on previous measurements.

For low-loaded filters and for sites with limited filter availability such as the Arctic, linear slope correction with multiple EC yield measurements can be a particular challenge. Here, we apply an optimised approach, using COMPYCALC that combines the determination of both EC losses and EC bias from charring of OC with the thermal-desorption model (Sect. 2.10). Furthermore, COMPYCALC uses the basis of Zhang et al. (2012) for the EC yield calculation and the charring calculation, where the attenuation (ATN, Sect. 2.10) calculated from the laser transmission signal is used. Charring correction after EC yield extrapolation was performed in accordance with Zotter et al. (2014), assuming that half of the pyrolytic EC that forms during the analysis is lost by the last heating step during WINSOC removal, complemented by a correction that considers different sensitivities of the ATN determination towards PC and EC; see Eqs. (10) and (11) in Sect. 2.10. Table 4 summarises EC and OC before and after corrections for EC yield and charring. The initial  $F^{14}\text{C}(\text{OC})$

value ( $F_{\text{OC}}$ ) is calculated with the initial EC value ( $F_{\text{EC}}$ ) for correction. As described in Sect. 2.10, the COMPYCALC script is run for the extrapolation of EC yield and charring correction to yield the final corrected EC value ( $F_{\text{EC}(\text{final})}$ ). Then, using  $F_{\text{EC}(\text{final})}$ , the final OC value ( $F_{\text{OC}(\text{final})}$ ) is calculated.

#### 3.4.2 Quality aspects of the $F^{14}\text{C}(\text{OC})$ calculation

Thermal-optical OC/EC separation discussed in the present work focuses on EC and WSOC and the optimisation thereof. Early work on  $^{14}\text{C}$  analysis did not include measures to reduce charring, which included substantial biases in the  $^{14}\text{C}$  analysis, particularly for EC but also for OC, as  $^{14}\text{C}(\text{OC})$  was determined directly by combustion of the filters in oxygen at  $340^\circ\text{C}$  (Szidat et al., 2004b). Later work included water extraction for charring reduction of EC (Yu et al., 2002; Novakov and Corrigan, 1995). Zhang et al. (2012) combined water extraction with an optimised four-step protocol and, thus, further improved OC/EC separation. However, only S1 was considered pure OC in this first TOA protocol and thus may include two possible biases of the  $^{14}\text{C}(\text{OC})$  result, as different OC fractions were not considered: first, the portion of OC that undergoes charring in S1 and, thus, is shifted to later steps and, second, more refractory OC that evolves during S2 and S3. This flaw was improved later by Zhang et al. (2015) by omitting the direct  $^{14}\text{C}$  measurement of OC, calculating  $F^{14}\text{C}(\text{OC})$  as the difference between  $F^{14}\text{C}(\text{TC})$  and  $F^{14}\text{C}(\text{EC})$ , as it is in the present study (Eq. 7). Hence, a better OC/EC separation improves both the quality of the measured  $F^{14}\text{C}(\text{EC})$  value and the calculated  $F^{14}\text{C}(\text{OC})$  value.

#### 3.4.3 Measurement limitations

Radiocarbon measurement requires a minimum of  $2\text{--}3 \mu\text{g C}$  per sample disregarding the hyphenation method (Wacker et al., 2013). With the setup used in the present work, the water extraction method is limited by extraction setup diameter and the number of punches to be stacked. Accordingly, for WSOC a minimum filter loading of  $0.3 \mu\text{g C cm}^{-2}$  is required. Within reason, there is no known limit for the chemical wet oxidation. Radiocarbon measurements coupled with the Sunset OC/EC analyser are limited by the sample holder, allowing for stacking of up to six rectangular  $1.5 \text{ cm}^2$  filter punches ( $9 \text{ cm}^2$  in total). In the present work, the remains after punching out the circular filters for WSOC were used for TC, which makes it difficult to fit the material on the regular sample holder. For pooled samples, the filter area used for TC was  $10.4 \text{ cm}^2$ , slightly exceeding the  $9 \text{ cm}^2$  limit. Therefore, for TC combustion we used a custom-built quartz spoon, on which up to  $16 \text{ cm}^2$  of filter material can be placed and combusted. Filter stacking must be omitted for  $^{14}\text{C}(\text{WINSOC})$  measurement. For this reason, filter loadings for S1 (pure WINSOC) of the Swiss\_4S protocol must be  $> 2 \mu\text{g C cm}^{-2}$ .

**Table 4.** Radiocarbon values for EC and OC before (i.e.  $F_{\text{EC}}$  and  $F_{\text{OC}}$ , respectively) and after the COMPYCALC extrapolation (i.e.  $F_{\text{EC}(\text{final})}$  and  $F_{\text{OC}(\text{final})}$ , respectively).

Start date	End date	$F_{\text{EC}}$ $F^{14}\text{C}$	$F_{\text{EC}(\text{final})}$ $F^{14}\text{C}$	$F_{\text{OC}}$ $F^{14}\text{C}$	$F_{\text{OC}(\text{final})}$ $F^{14}\text{C}$
23 February 2017	2 March 2017	0.881	0.917	0.749	0.743
5 May 2017	15 May 2017	0.597	0.656	1.165	1.153
31 May 2017	26 June 2017	0.642	0.699	0.951	0.924
8 September 2017*	28 September 2017	0.689	0.735	0.993	0.987
28 September 2017	6 October 2017	0.544	0.620	1.095	1.086
6 October 2017*	24 October 2017	0.748	0.801	0.837	0.829
5 December 2017*	21 December 2017	0.563	0.612	0.492	0.475
23 January 2018	31 January 2018	0.184	0.226	0.652	0.643
21 March 2018	29 March 2018	0.570	0.618	1.014	1.006
6 April 2018	16 April 2018	0.527	0.591	1.027	1.016
12 July 2018*	30 July 2018	0.677	0.717	0.802	0.796
30 July 2018*	15 August 2018	0.767	0.794	1.011	1.009
23 November 2018	3 December 2018	0.554	0.633	0.756	0.743

\* Pooled filters.

The  $^{14}\text{C}$ (WINSOC) measurements were omitted in the current study, as only 4 of the 13 samples had a filter loading  $> 2 \mu\text{g C cm}^{-2}$ , with a mean loading of  $1.8 \mu\text{g C cm}^{-2}$  (range:  $0.9\text{--}5 \mu\text{g C cm}^{-2}$ ).

### 3.4.4 Radiocarbon results

Radiocarbon measurements of TC show a larger input from fossil carbon in winter months relative to the summer months with an average  $F^{14}\text{C}$  of  $0.85 \pm 0.17$  (Table 5).  $F^{14}\text{C}$  values close to non-fossil levels of radiocarbon were found for spring, summer, and autumn with an average  $F^{14}\text{C}$  of  $0.95 \pm 0.09$  and the highest levels in spring and late summer. Large variations in  $^{14}\text{C}$ (EC) were observed, ranging from 0.23 to 0.92 (mean:  $0.66 \pm 0.16$ ). Both the highest and the lowest value were observed in winter (23 February–2 March 2017 and 23–31 January 2018), showing that the relative source composition of Arctic carbonaceous aerosol can vary widely within a season. The highest  $^{14}\text{C}$ (EC) value had the second-highest EC concentration ( $40 \text{ ng C m}^{-3}$ ) and an OC/EC ratio of 5.4, whereas the sample with the very low fraction modern carbon had an EC concentration of  $16 \text{ ng C m}^{-3}$  and OC/EC ratio of 9.6. Notably, the  $^{14}\text{C}$ (WSOC) content of the high fraction modern carbon sample (1.077) was substantially higher than that of EC, indicating different sources of WSOC and EC. Overall,  $^{14}\text{C}$ (WSOC) values showed non-fossil levels of radiocarbon with maxima in spring and late summer and lower values in early summer and winter.

Some  $^{14}\text{C}$  measurements of EC have already been performed at the Zeppelin Observatory. Winiger et al. (2015) investigated 14 winter samples from January–March 2009 and observed an average fraction of biomass burning ( $f_{\text{bb}}$ ) of  $0.60 \pm 0.21$ . Later, Winiger et al. (2019) analysed 11 sam-

ples from late 2012 to late 2013, which can be classified into 6 winter samples from November 2012 to March 2013 as well as November to December 2013 and 3 summer samples from April to early November 2013. Whereas the winter samples showed  $f_{\text{bb}}$  values of  $0.37 \pm 0.03$ , indicating a much higher fossil contribution compared to their results from 4 years before and a small variability between the samples, the summer samples revealed a larger scatter with  $f_{\text{bb}}$  values of  $0.54 \pm 0.11$ . In order to compare our measurement with these two studies, we converted  $^{14}\text{C}$ (EC) results into  $f_{\text{bb}}$  values using conversion factors of 1.084 and 1.080 for 2017 and 2018, respectively, based on the approach described in Zotter et al. (2014), providing  $0.59 \pm 0.24$  and  $0.63 \pm 0.06$  for winter and summer, respectively. Our values for summer (i.e. April–October) correspond very well with the summer data from 2013 by Winiger et al. (2019). For the winter data, our results from November to March compare well with the measurements for 2009 from Winiger et al. (2015), whereas there is a large discrepancy of the dataset from 2012/13 from Winiger et al. (2019) with both our outcome and the study of Winiger et al. (2015). This comparison suggests that two substantial changes have occurred from 2009 to 2012/2013 from wood-burning-dominated to fossil-fuel-combustion-dominated EC sources and from 2012/13 to 2017–2018 back to wood-burning-dominated emissions. The discussion and interpretation of this result are beyond the scope of this work. We nevertheless emphasise that the EC isolation procedure of Winiger et al. (2015, 2019) neither involved water extraction nor applied oxygen in the OC removal steps, so these datasets should be compared with caution with our results.

**Table 5.** Final radiocarbon results for each fraction after all calculations and corrections described in this work.

Start date	End date	TC $F^{14}\text{C}$	EC <sub>final</sub> $F^{14}\text{C}$	WSOC $F^{14}\text{C}$	OC <sub>final</sub> $F^{14}\text{C}$
23 February 2017	2 March 2017	0.770	0.917	0.818	0.743
5 May 2017	15 May 2017	1.068	0.656	0.987	1.153
31 May 2017	26 June 2017	0.852	0.699	**	0.924
8 September 2017*	28 September 2017	0.959	0.735	0.975	0.987
28 September 2017	6 October 2017	1.036	0.620	0.929	1.086
6 October 2017*	24 October 2017	0.825	0.801	0.795	0.829
5 December 2017*	21 December 2017	0.509	0.612	0.758***	0.475
23 January 2018	31 January 2018	0.573	0.226	0.841	0.643
21 March 2018	29 March 2018	0.951	0.618	1.077	1.006
6 April 2018	16 April 2018	0.957	0.591	0.652	1.016
12 July 2018*	30 July 2018	0.786	0.717	0.792	0.796
30 July 2018*	15 August 2018	0.997	0.794	1.055	1.009
23 November 2018	3 December 2018	0.727	0.633	0.666	0.743

\* Pooled filters.

\*\* Not measurable due to too low WSOC amount.

\*\*\* Only one of the pooled samples (i.e. 5–13 December 2017) was considered as the other one (i.e. 13–21 December 2017) was not measurable due to too low WSOC amount.

## 4 Conclusions

In the current study, we present an optimised separation procedure for radiocarbon measurements of TC, EC, and WSOC. Prior to thermal–optical OC/EC separation, a water extraction step was used to minimise charring and to provide eluates for  $^{14}\text{C}$ (WSOC) measurement. Our method enables radiocarbon source apportionment of the EC and WSOC fraction in addition to TC and, when sufficiently loaded filters are available, also the WINSOC fraction. Furthermore, the fraction modern of the OC can be calculated from these values. Prior to AMS  $^{14}\text{C}$  analysis, combustion of TC, EC, and WINSOC are all performed with a Sunset OC/EC analyser, simplifying the measurement by using a single hyphenation device for multiple carbonaceous fractions. Lacking standard reference material for atmospheric EC on filters, we chose thoroughly analysed and well-homogenised high-volume filters for method validation. As demonstrated for low-loaded Arctic filters, chemical wet oxidation is a simple and reliable method for measurement of the WSOC fraction, providing low procedural blanks. Intercomparison with other methodologies is pending. Furthermore, complete method validation is not feasible due to the unavailability of suitable reference material. Due to this situation, method validation may still be more effective today if based on thoroughly analysed and well-homogenised high-volume filters.

We have developed a web tool for calculation of both amount and EC yield, named Sunset-calc, allowing an EC yield calculation after each run and providing the fraction of charring for each step in the Swiss\_3S protocol. Sunset-calc enables rapid protocol optimisations for a low fraction of charring while avoiding too large EC losses before the S4 step.

Our thermal-desorption model approach for EC yield extrapolation provides a filter-specific non-linear correction based on the underlying physical properties of the OC/EC mixture and OC composition. The present method is a major leap forward in  $^{14}\text{C}$ (EC) correction calculation and supersedes the currently used linear approach for EC yield extrapolation. Radiocarbon measurements using filters with deliberately lowered EC yields are no longer necessary. Our approach is independent of season and does not require additional filter material for EC yield extrapolation, which is crucial when only limited amounts of sample material are available.

**Code availability.** The codes are available at <https://doi.org/10.5281/zenodo.6148364> (Rauber and Straehl, 2022) and <https://doi.org/10.5281/zenodo.7368424> (Rauber and Salazar, 2022).

**Data availability.** Data in the figures are available in the Zenodo repository: <https://doi.org/10.5281/zenodo.7612886> (Rauber, 2023).

**Supplement.** The supplement related to this article is available online at: <https://doi.org/10.5194/amt-16-825-2023-supplement>.

**Author contributions.** The work presented here was carried out in collaboration between all authors. SS conceived of the study and its design. MR performed the laboratory experiments, implemented the models, and led the preparation of the manuscript. GS created the models, provided guidance and supervision for the laboratory ex-



periments and model implementation, and contributed to the preparation of the manuscript. KEY was responsible for collection of the aerosol filter samples and for determining their OC, EC, and TC content. All authors contributed to the editing and proofreading of the manuscript.

*Competing interests.* The contact author has declared that none of the authors has any competing interests.

*Disclaimer.* Publisher's note: Copernicus Publications remains neutral with regard to jurisdictional claims in published maps and institutional affiliations.

*Acknowledgements.* We would like to thank Jan Str hl for his contribution to the Sunset-calc application and Ren  Bleisch for setting up the R server.

*Financial support.* This research has been supported by the Norwegian Ministry of Climate and Environment.

*Review statement.* This paper was edited by Pierre Herckes and reviewed by Sanjeev Dasari and one anonymous referee.

## References

- Abbatt, J. P. D., Leaitch, W. R., Aliabadi, A. A., Bertram, A. K., Blanchet, J.-P., Boivin-Rioux, A., Bozem, H., Burkart, J., Chang, R. Y. W., Charette, J., Chaubey, J. P., Christensen, R. J., Cirisan, A., Collins, D. B., Croft, B., Dionne, J., Evans, G. J., Fletcher, C. G., Gal , M., Ghahreman, R., Girard, E., Gong, W., Gosselin, M., Gourdal, M., Hanna, S. J., Hayashida, H., Herber, A. B., Hesarakis, S., Hoor, P., Huang, L., Husherr, R., Irish, V. E., Keita, S. A., Kodros, J. K., K llner, F., Kolonjari, F., Kunkel, D., Ladino, L. A., Law, K., L vasseur, M., Libois, Q., Liggio, J., Lizotte, M., Macdonald, K. M., Mahmood, R., Martin, R. V., Mason, R. H., Miller, L. A., Moravek, A., Mortenson, E., Mungall, E. L., Murphy, J. G., Namazi, M., Norman, A.-L., O'Neill, N. T., Pierce, J. R., Russell, L. M., Schneider, J., Schulz, H., Sharma, S., Si, M., Staebler, R. M., Steiner, N. S., Thomas, J. L., von Salzen, K., Wentzell, J. J. B., Willis, M. D., Wentworth, G. R., Xu, J.-W., and Yakobi-Hancock, J. D.: Overview paper: New insights into aerosol and climate in the Arctic, *Atmos. Chem. Phys.*, 19, 2527–2560, <https://doi.org/10.5194/acp-19-2527-2019>, 2019.
- Agrios, K., Salazar, G., Zhang, Y.-L., Uglietti, C., Battaglia, M., Luginb hl, M., Ciobanu, V. G., Vonwiller, M., and Szidat, S.: Online coupling of pure O<sub>2</sub> thermo-optical methods – <sup>14</sup>C AMS for source apportionment of carbonaceous aerosols, *Instrum. Meth. B*, 361, 288–293, <https://doi.org/10.1016/j.nimb.2015.06.008>, 2015.
- Andersson, A., Sheesley, R. J., Krus , M., Johansson, C., and Gustafsson,  .: <sup>14</sup>C-Based source assessment of soot aerosols in Stockholm and the Swedish EMEP-Aspvreten regional background site, *Atmos. Environ.*, 45, 215–222, <https://doi.org/10.1016/j.atmosenv.2010.09.015>, 2011.
- Barrett, T. E., Robinson, E. M., Usenko, S., and Sheesley, R. J.: Source Contributions to Wintertime Elemental and Organic Carbon in the Western Arctic Based on Radiocarbon and Tracer Apportionment, *Environ. Sci. Technol.*, 49, 11631–11639, <https://doi.org/10.1021/acs.est.5b03081>, 2015.
- Barrie, L. A.: Arctic air pollution: An overview of current knowledge, *Atmos. Environ.*, 20, 643–663, [https://doi.org/10.1016/0004-6981\(86\)90180-0](https://doi.org/10.1016/0004-6981(86)90180-0), 1986.
- Barrie, L. A., Hoff, R. M., and Daggupaty, S. M.: The influence of mid-latitude pollution sources on haze in the Canadian arctic, *Atmos. Environ.*, 15, 1407–1419, [https://doi.org/10.1016/0004-6981\(81\)90347-4](https://doi.org/10.1016/0004-6981(81)90347-4), 1981.
- Baumgardner, D., Popovicheva, O., Allan, J., Bernardoni, V., Cao, J., Cavalli, F., Cozic, J., Diapouli, E., Eleftheriadis, K., Genberg, P. J., Gonzalez, C., Gysel, M., John, A., Kirchstetter, T. W., K hlbusch, T. A. J., Laborde, M., Lack, D., M ller, T., Niessner, R., Petzold, A., Piazzalunga, A., Putaud, J. P., Schwarz, J., Sheridan, P., Subramanian, R., Swietlicki, E., Valli, G., Vecchi, R., and Viana, M.: Soot reference materials for instrument calibration and intercomparisons: a workshop summary with recommendations, *Atmos. Meas. Tech.*, 5, 1869–1887, <https://doi.org/10.5194/amt-5-1869-2012>, 2012.
- Bedjanian, Y., Nguyen, M. L., and Guilloteau, A.: Desorption of Polycyclic Aromatic Hydrocarbons from Soot Surface: Five- and Six-Ring (C<sub>22</sub>, C<sub>24</sub>) PAHs, *J. Phys. Chem. A*, 114, 3533–3539, <https://doi.org/10.1021/jp912110b>, 2010.
- Bernardoni, V., Calzolari, G., Chiari, M., Fedi, M., Lucarelli, F., Nava, S., Piazzalunga, A., Riccobono, F., Taccetti, F., Valli, G., and Vecchi, R.: Radiocarbon analysis on organic and elemental carbon in aerosol samples and source apportionment at an urban site in Northern Italy, *J. Aerosol Sci.*, 56, 88–99, <https://doi.org/10.1016/j.jaerosci.2012.06.001>, 2013.
- Birch, M. E. and Cary, R. A.: Elemental Carbon-Based Method for Monitoring Occupational Exposures to Particulate Diesel Exhaust, *Aerosol Sci. Tech.*, 25, 221–241, <https://doi.org/10.1080/02786829608965393>, 1996.
- Bond, T. C., Doherty, S. J., Fahey, D. W., Forster, P. M., Berntsen, T., Deangelo, B. J., Flanner, M. G., Ghan, S., K rcher, B., Koch, D., Kinne, S., Kondo, Y., Quinn, P. K., Sorooshian, M. C., Schultz, M. G., Schulz, M., Venkataraman, C., Zhang, H., Zhang, S., Bellouin, N., Guttikunda, S. K., Hopke, P. K., Jacobson, M. Z., Kaiser, J. W., Klimont, Z., Lohmann, U., Schwarz, J. P., Shindell, D., Storelvmo, T., Warren, S. G., and Zender, C. S.: Bounding the role of black carbon in the climate system: A scientific assessment, *J. Geophys. Res.-Atmos.*, 118, 5380–5552, <https://doi.org/10.1002/jgrd.50171>, 2013.
- Boparai, P., Lee, J., and Bond, T. C.: Revisiting thermal-optical analyses of carbonaceous aerosol using a physical model, *Aerosol Sci. Tech.*, 42, 930–948, <https://doi.org/10.1080/02786820802360690>, 2008.
- Cadle, S. H., Groblicki, P. J., and Stroup, D. P.: Automated Carbon Analyzer For Particulate Samples, *Anal. Chem.*, 52, 2201–2206, <https://doi.org/10.1021/ac50063a047>, 1980.
- Cavalli, F., Viana, M., Yttri, K. E., Genberg, J., and Putaud, J.-P.: Toward a standardised thermal-optical protocol for measuring atmospheric organic and elemental carbon: the EUSAAR protocol,

- Atmos. Meas. Tech., 3, 79–89, <https://doi.org/10.5194/amt-3-79-2010>, 2010.
- Chang, W., Cheng, J., Allaire, J., Sievert, C., Schloerke, B., Xie, Y., Allen, J., McPherson, J., Dipert, A., and Borges, B.: shiny: Web Application Framework for R, R package version 1.7.4.9002, <https://shiny.rstudio.com/> (last access: 27 January 2023), 2017.
- Chow, J. C., Watson, J. G., Pritchett, L. C., Pierson, W. R., Frazier, C. A., and Purcell, R. G.: The DRI thermal/optical reflectance carbon analysis system: description, evaluation and applications in U.S. Air quality studies, *Atmos. Environ. A Gen.*, 27, 1185–1201, [https://doi.org/10.1016/0960-1686\(93\)90245-T](https://doi.org/10.1016/0960-1686(93)90245-T), 1993.
- Chow, J. C., Watson, J. G., Chen, L. W. A., Arnott, W. P., Moosmüller, H., and Fung, K.: Equivalence of elemental carbon by thermal/optical reflectance and transmittance with different temperature protocols, *Environ. Sci. Technol.*, 38, 4414–4422, <https://doi.org/10.1021/es034936u>, 2004.
- Contini, D., Vecchi, R., and Viana, M.: Carbonaceous Aerosols in the Atmosphere, *Atmosphere (Basel)*, 9, 181, <https://doi.org/10.3390/atmos9050181>, 2018.
- Daellenbach, K. R., Uzu, G., Jiang, J., Cassagnes, L.-E., Leni, Z., Vlachou, A., Stefanelli, G., Canonaco, F., Weber, S., Segers, A., Kuenen, J. J. P., Schaap, M., Favez, O., Albinet, A., Aksoyoglu, S., Dommen, J., Baltensperger, U., Geiser, M., El Haddad, I., Jaffrezo, J.-L., and Prévôt, A. S. H.: Sources of particulate-matter air pollution and its oxidative potential in Europe, *Nature*, 587, 414–419, <https://doi.org/10.1038/s41586-020-2902-8>, 2020.
- Dasari, S. and Widory, D.: Radiocarbon ( $^{14}\text{C}$ ) Analysis of Carbonaceous Aerosols: Revisiting the Existing Analytical Techniques for Isolation of Black Carbon, *Front. Environ. Sci.*, 10, 907467, <https://doi.org/10.3389/fenvs.2022.907467>, 2022.
- Dusek, U., Monaco, M., Prokopiou, M., Gongriep, F., Hitzenberger, R., Meijer, H. A. J., and Röckmann, T.: Evaluation of a two-step thermal method for separating organic and elemental carbon for radiocarbon analysis, *Atmos. Meas. Tech.*, 7, 1943–1955, <https://doi.org/10.5194/amt-7-1943-2014>, 2014.
- Eller, P. M. and Cassinelli, M. E.: Niosh, Elemental Carbon (Diesel Particulate): Method 5040, NIOSH Manual of Analytical Methods (NMAM), Natl. Inst. Occup. Saf. Heal. Cincinnati, OH, USA, 2003–2154, <https://www.cdc.gov/niosh/docs/2003-154/pdfs/5040f3.pdf> (last access: 27 January 2023), 1996.
- Engelmann, R., Ansmann, A., Ohneiser, K., Griesche, H., Radenz, M., Hofer, J., Althausen, D., Dahlke, S., Maturilli, M., Veselovskii, I., Jimenez, C., Wiesen, R., Baars, H., Bühl, J., Gebauer, H., Haarig, M., Seifert, P., Wandinger, U., and Macke, A.: Wildfire smoke, Arctic haze, and aerosol effects on mixed-phase and cirrus clouds over the North Pole region during MO-SAiC: an introduction, *Atmos. Chem. Phys.*, 21, 13397–13423, <https://doi.org/10.5194/acp-21-13397-2021>, 2021.
- Fahrni, S. M., Wacker, L., Synal, H. A., and Szidat, S.: Improving a gas ion source for  $^{14}\text{C}$  AMS, *Nucl. Instrum. Meth. B*, 294, 320–327, <https://doi.org/10.1016/j.nimb.2012.03.037>, 2013.
- GBD 2015 Risk Factors Collaborators: Global, regional, and national comparative risk assessment of 79 behavioural, environmental and occupational, and metabolic risks or clusters of risks, 1990–2015: a systematic analysis for the Global Burden of Disease Study 2015, *Lancet*, 388, 1659–1724, [https://doi.org/10.1016/S0140-6736\(16\)31679-8](https://doi.org/10.1016/S0140-6736(16)31679-8), 2016.
- Gentner, D. R., Jathar, S. H., Gordon, T. D., Bahreini, R., Day, D. A., El Haddad, I., Hayes, P. L., Pieber, S. M., Platt, S. M., De Gouw, J., Goldstein, A. H., Harley, R. A., Jimenez, J. L., Prévôt, A. S. H., and Robinson, A. L.: Review of Urban Secondary Organic Aerosol Formation from Gasoline and Diesel Motor Vehicle Emissions, *Environ. Sci. Technol.*, 51, 1074–1093, <https://doi.org/10.1021/acs.est.6b04509>, 2017.
- Ghosh, U., Talley, J. W., and Luthy, R. G.: Particle-Scale Investigation of PAH Desorption Kinetics and Thermodynamics from Sediment, *Environ. Sci. Technol.*, 35, 3468–3475, <https://doi.org/10.1021/es0105820>, 2001.
- Glatzel, S. and Well, R.: Evaluation of septum-capped vials for storage of gas samples during air transport, *Environ. Monit. Assess.*, 136, 307–311, <https://doi.org/10.1007/s10661-007-9686-2>, 2008.
- Gundel, L. A., Dod, R. L., Rosen, H., and Novakov, T.: the Relationship Between Optical Attenuation and Black Carbon, *Sci. Total Environ.*, 36, 197–202, 1984.
- Gustafsson, Ö., Bucheli, T. D., Kukulska, Z., Andersson, M., Largeau, C., Rouzaud, J. N., Reddy, C. M., and Eglinton, T. I.: Evaluation of a protocol for the quantification of black carbon in sediments, *Global Biogeochem. Cy.*, 15, 881–890, <https://doi.org/10.1029/2000GB001380>, 2001.
- Hanke, U. M., Wacker, L., Haghipour, N., Schmidt, M. W. I., Eglinton, T. I., and McIntyre, C. P.: Comprehensive radiocarbon analysis of benzene polycarboxylic acids (BPCAs) derived from pyrogenic carbon in environmental samples, *Radiocarbon*, 59, 1103–1116, <https://doi.org/10.1017/RDC.2017.44>, 2017.
- Heidam, N. Z., Christensen, J., Wählin, P., and Skov, H.: Arctic atmospheric contaminants in NE Greenland: Levels, variations, origins, transport, transformations and trends 1990–2001, *Sci. Total Environ.*, 331, 5–28, <https://doi.org/10.1016/j.scitotenv.2004.03.033>, 2004.
- Hung, H., Kallenborn, R., Breivik, K., Su, Y., Brorström-Lundén, E., Olafsdottir, K., Thorlacius, J. M., Leppänen, S., Bossi, R., Skov, H., Manø, S., Patton, G. W., Stern, G., Sverko, E., and Fellin, P.: Atmospheric monitoring of organic pollutants in the Arctic under the Arctic Monitoring and Assessment Programme (AMAP): 1993–2006, *Sci. Total Environ.*, 408, 2854–2873, <https://doi.org/10.1016/j.scitotenv.2009.10.044>, 2010.
- Huntzicker, J. J., Johnson, R. L., Shah, J. J., and Cary, R. A.: Analysis of Organic and Elemental Carbon in Ambient Aerosols by a Thermal-Optical Method, in: *Particulate Carbon: Atmospheric Life Cycle*, edited by: Wolff, G. T. and Klimisch, R. L., Springer US, Boston, MA, 79–88, [https://doi.org/10.1007/978-1-4684-4154-3\\_6](https://doi.org/10.1007/978-1-4684-4154-3_6), 1982.
- IPCC: Climate Change 2021: The Physical Science Basis. Contribution of Working Group I to the Sixth Assessment Report of the Intergovernmental Panel on Climate Change, Cambridge University Press, 2021.
- Jenk, T. M., Szidat, S., Schwikowski, M., Gäggeler, H. W., Wacker, L., Synal, H.-A., and Saurer, M.: Microgram level radiocarbon ( $^{14}\text{C}$ ) determination on carbonaceous particles in ice, *Nucl. Instrum. Meth. B*, 259, 518–525, <https://doi.org/10.1016/j.nimb.2007.01.196>, 2007.
- Jouan, C., Pelon, J., Girard, E., Ancellet, G., Blanchet, J. P., and Delanoë, J.: On the relationship between Arctic ice clouds and polluted air masses over the North Slope of Alaska in April 2008, *Atmos. Chem. Phys.*, 14, 1205–1224, <https://doi.org/10.5194/acp-14-1205-2014>, 2014.

- Kanakidou, M., Seinfeld, J. H., Pandis, S. N., Barnes, I., Dentener, F. J., Facchini, M. C., Van Dingenen, R., Ervens, B., Nenes, A., Nielsen, C. J., Swietlicki, E., Putaud, J. P., Balkanski, Y., Fuzzi, S., Horth, J., Moortgat, G. K., Winterhalter, R., Myhre, C. E. L., Tsigaridis, K., Vignati, E., Stephanou, E. G., and Wilson, J.: Organic aerosol and global climate modelling: a review, *Atmos. Chem. Phys.*, 5, 1053–1123, <https://doi.org/10.5194/acp-5-1053-2005>, 2005.
- Keeling, C. D.: The concentration and isotopic abundances of atmospheric carbon dioxide in rural areas, *Geochim. Cosmochim. Acta*, 13, 322–334, [https://doi.org/10.1016/0016-7037\(58\)90033-4](https://doi.org/10.1016/0016-7037(58)90033-4), 1958.
- Kim, K. H., Jahan, S. A., Kabir, E., and Brown, R. J. C.: A review of airborne polycyclic aromatic hydrocarbons (PAHs) and their human health effects, *Environ. Int.*, 60, 71–80, <https://doi.org/10.1016/j.envint.2013.07.019>, 2013.
- Kim, K. H., Kabir, E., and Kabir, S.: A review on the human health impact of airborne particulate matter, *Environ. Int.*, 74, 136–143, <https://doi.org/10.1016/j.envint.2014.10.005>, 2015.
- Kirillova, E. N., Andersson, A., Sheesley, R. J., Kruså, M., Praveen, P. S., Budhavant, K., Safai, P. D., Rao, P. S. P., and Gustafsson, Ö.: <sup>13</sup>C- and <sup>14</sup>C-based study of sources and atmospheric processing of water-soluble organic carbon (WSOC) in South Asian aerosols, *J. Geophys. Res.-Atmos.*, 118, 614–626, <https://doi.org/10.1002/jgrd.50130>, 2013.
- Landrigan, P. J.: Air pollution and health, *Lancet Public Heal.*, 2, e4–e5, [https://doi.org/10.1016/S2468-2667\(16\)30023-8](https://doi.org/10.1016/S2468-2667(16)30023-8), 2017.
- Lang, S. Q., Bernasconi, S. M., and Fröh-Green, G. L.: Stable isotope analysis of organic carbon in small (µgC) samples and dissolved organic matter using a GasBench preparation device, *Rapid Commun. Mass Sp.*, 26, 9–16, <https://doi.org/10.1002/rcm.5287>, 2012.
- Lang, S. Q., Fröh-Green, G. L., Bernasconi, S. M., and Wacker, L.: Isotopic ( $\delta^{13}\text{C}$ ,  $\Delta^{14}\text{C}$ ) analysis of organic acids in marine samples using wet chemical oxidation, *Limnol. Oceanogr.-Meth.*, 11, 161–175, <https://doi.org/10.4319/lom.2013.11.161>, 2013.
- Lelieveld, J., Evans, J. S., Fnais, M., Giannadaki, D., and Pozzer, A.: The contribution of outdoor air pollution sources to premature mortality on a global scale, *Nature*, 525, 367–371, <https://doi.org/10.1038/nature15371>, 2015.
- Mauderly, J. L. and Chow, J. C.: Health Effects of Organic Aerosols, *Inhal. Toxicol.*, 20, 257–288, <https://doi.org/10.1080/08958370701866008>, 2008.
- McDow, S. R. and Huntzicker, J. J.: Vapor adsorption artifact in the sampling of organic aerosol: Face velocity effects, *Atmos. Environ. A Gen.*, 24, 2563–2571, [https://doi.org/10.1016/0960-1686\(90\)90134-9](https://doi.org/10.1016/0960-1686(90)90134-9), 1990.
- McNeill, V. F.: Atmospheric Aerosols: Clouds, Chemistry, and Climate, *Annu. Rev. Chem. Biomol.*, 8, 427–444, <https://doi.org/10.1146/annurev-chembioeng-060816-101538>, 2017.
- Menzel, D. W. and Vaccaro, R. F.: The measurement of dissolved organic and particulate carbon in seawater, *Limnol. Oceanogr.*, 9, 138–142, <https://doi.org/10.4319/lo.1964.9.1.0138>, 1964.
- Moschos, V., Gysel-Beer, M., Modini, R. L., Corbin, J. C., Massabò, D., Costa, C., Danelli, S. G., Vlachou, A., Daellenbach, K. R., Szidat, S., Prati, P., Prévôt, A. S. H., Baltensperger, U., and El Haddad, I.: Source-specific light absorption by carbonaceous components in the complex aerosol matrix from yearly filter-based measurements, *Atmos. Chem. Phys.*, 21, 12809–12833, <https://doi.org/10.5194/acp-21-12809-2021>, 2021.
- Moschos, V., Dzepina, K., Bhattu, D., Lamkaddam, H., Casotto, R., Daellenbach, K. R., Canonaco, F., Rai, P., Aas, W., Becagli, S., Calzolari, G., Eleftheriadis, K., Moffett, C. E., Schnelle-Kreis, J., Severi, M., Sharma, S., Skov, H., Vestenius, M., Zhang, W., Hakola, H., Hellén, H., Huang, L., Jaffrezo, J.-L., Massling, A., Nøjgaard, J. K., Petäjä, T., Popovicheva, O., Sheesley, R. J., Traversi, R., Yttri, K. E., Schmale, J., Prévôt, A. S. H., Baltensperger, U., and El Haddad, I.: Equal abundance of summertime natural and wintertime anthropogenic Arctic organic aerosols, *Nat. Geosci.*, 15, 196–202, <https://doi.org/10.1038/s41561-021-00891-1>, 2022.
- Novakov, T. and Corrigan, C. E.: Mikrochimica Acta Thermal Characterization of Biomass Smoke Particles, *Mikrochim. Acta*, 166, 157–166, 1995.
- Peleg, M., Normand, M. D., and Corradini, M. G.: The Arrhenius Equation Revisited, *Crit. Rev. Food Sci.*, 52, 830–851, <https://doi.org/10.1080/10408398.2012.667460>, 2012.
- Peterson, M. R. and Richards, M. H.: Thermal-optical-transmittance analysis for organic, elemental, carbonate, total carbon, and OCX2 in PM2.5 by the EPA/NIOSH method, in: *Proceedings, Symposium on Air Quality Measurement Methods and Technology – 2002*, Pittsburgh, PA, 83-1–83-19, [https://hero.epa.gov/hero/index.cfm/reference/details/reference\\_id/156861](https://hero.epa.gov/hero/index.cfm/reference/details/reference_id/156861) (last access: 27 January 2023), 2002.
- Petzold, A., Ogren, J. A., Fiebig, M., Laj, P., Li, S.-M., Baltensperger, U., Holzer-Popp, T., Kinne, S., Pappalardo, G., Sugimoto, N., Wehrli, C., Wiedensohler, A., and Zhang, X.-Y.: Recommendations for reporting “black carbon” measurements, *Atmos. Chem. Phys.*, 13, 8365–8379, <https://doi.org/10.5194/acp-13-8365-2013>, 2013.
- Platt, S. M., Hov, Ø., Berg, T., Breivik, K., Eckhardt, S., Eleftheriadis, K., Evangeliou, N., Fiebig, M., Fisher, R., Hansen, G., Hansson, H.-C., Heintzenberg, J., Hermansen, O., Heslin-Rees, D., Holmén, K., Hudson, S., Kallenborn, R., Krejci, R., Krognes, T., Larssen, S., Lowry, D., Lund Myhre, C., Lunder, C., Nisbet, E., Nizzetto, P. B., Park, K.-T., Pedersen, C. A., Aspmo Pfaffhuber, K., Röckmann, T., Schmidbauer, N., Solberg, S., Stohl, A., Ström, J., Svendby, T., Tunved, P., Tørnkvis, K., van der Veen, C., Vratolis, S., Yoon, Y. J., Yttri, K. E., Zieger, P., Aas, W., and Tørseth, K.: Atmospheric composition in the European Arctic and 30 years of the Zeppelin Observatory, Ny-Ålesund, *Atmos. Chem. Phys.*, 22, 3321–3369, <https://doi.org/10.5194/acp-22-3321-2022>, 2022.
- Pope, C. A., Coleman, N., Pond, Z. A., and Burnett, R. T.: Fine particulate air pollution and human mortality: 25+ years of cohort studies, *Environ. Res.*, 183, 108924, <https://doi.org/10.1016/j.envres.2019.108924>, 2020.
- Pöschl, U.: Aerosol particle analysis: Challenges and progress, *Anal. Bioanal. Chem.*, 375, 30–32, <https://doi.org/10.1007/s00216-002-1611-5>, 2003.
- Putaud, J. P., Van Dingenen, R., Alastuey, A., Bauer, H., Birmili, W., Cyrys, J., Flentje, H., Fuzzi, S., Gehrig, R., Hansson, H. C., Harrison, R. M., Herrmann, H., Hiltnerberger, R., Hügl, C., Jones, A. M., Kasper-Giebl, A., Kiss, G., Kousa, A., Kuhlbusch, T. A. J., Löschau, G., Maenhaut, W., Molnar, A., Moreno, T., Pekkanen, J., Perrino, C., Pitz, M., Puxbaum, H., Querol, X., Rodriguez, S., Salma, I., Schwarz, J., Smolik, J., Schneider, J., Spindler, G., ten

- Brink, H., Tursic, J., Viana, M., Wiedensohler, A., and Raes, F.: A European aerosol phenomenology – 3: Physical and chemical characteristics of particulate matter from 60 rural, urban, and kerbside sites across Europe, *Atmos. Environ.*, 44, 1308–1320, <https://doi.org/10.1016/j.atmosenv.2009.12.011>, 2010.
- Quinn, P. K., Miller, T. L., Bates, T. S., Ogren, J. A., Andrews, E., and Shaw, G. E.: A 3-year record of simultaneously measured aerosol chemical and optical properties at Barrow, Alaska, *J. Geophys. Res.-Atmos.*, 107, AAC 8-1–AAC 8-15, <https://doi.org/10.1029/2001jd001248>, 2002.
- Quinn, P. K., Bates, T. S., Baum, E., Doubleday, N., Fiore, A. M., Flanner, M., Fridlind, A., Garrett, T. J., Koch, D., Menon, S., Shindell, D., Stohl, A., and Warren, S. G.: Short-lived pollutants in the Arctic: their climate impact and possible mitigation strategies, *Atmos. Chem. Phys.*, 8, 1723–1735, <https://doi.org/10.5194/acp-8-1723-2008>, 2008.
- R Core Team: R: A Language and Environment for Statistical Computing, R Foundation for Statistical Computing, Vienna, Austria, <https://www.r-project.org/> (last access: 26 January 2023), 2020.
- Rauber, M.: Dataset for: An optimised organic carbon/elemental carbon (OC/EC) fraction separation method for radiocarbon source apportionment applied to low-loaded Arctic aerosol filters, Zenodo [data set], <https://doi.org/10.5281/zenodo.7612886>, 2023.
- Rauber, M. and Salazar, G.: COMPYCALC, Version 1.3.0, Zenodo [code], <https://doi.org/10.5281/zenodo.7368424>, 2022.
- Rauber, M. and Straehl, J.: martin-rauber/sunset-calc, Version v1.0.2, Zenodo [code], <https://doi.org/10.5281/zenodo.6148364>, 2022.
- Ruff, M., Wacker, L., Gäggeler, H. W., Suter, M., Synal, H.-A., and Szidat, S.: A Gas Ion Source for Radiocarbon Measurements at 200 kV, *Radiocarbon*, 49, 307–314, <https://doi.org/10.1017/S0033822200042235>, 2007.
- Salazar, G., Zhang, Y. L., Agrios, K., and Szidat, S.: Development of a method for fast and automatic radiocarbon measurement of aerosol samples by online coupling of an elemental analyzer with a MICADAS AMS, *Nucl. Instrum. Meth. B*, 361, 163–167, <https://doi.org/10.1016/j.nimb.2015.03.051>, 2015.
- Schmale, J., Zieger, P., and Ekman, A. M. L.: Aerosols in current and future Arctic climate, *Nat. Clim. Change*, 11, 95–105, <https://doi.org/10.1038/s41558-020-00969-5>, 2021.
- Schmid, H., Laskus, L., Jürgen Abraham, H., Baltensperger, U., Lavanchy, V., Bizjak, M., Burba, P., Cachier, H., Crow, D., Chow, J., Gnauk, T., Even, A., Ten Brink, H. M., Giesen, K. P., Hitznerberger, R., Hueglin, C., Maenhaut, W., Pio, C., Carvalho, A., Putaud, J. P., Toom-Sauntry, D., and Puxbaum, H.: Results of the “carbon conference” international aerosol carbon round robin test stage I, *Atmos. Environ.*, 35, 2111–2121, [https://doi.org/10.1016/S1352-2310\(00\)00493-3](https://doi.org/10.1016/S1352-2310(00)00493-3), 2001.
- Schwaab, M. and Pinto, J. C.: Optimum reference temperature for reparameterization of the Arrhenius equation. Part 1: Problems involving one kinetic constant, *Chem. Eng. Sci.*, 62, 2750–2764, <https://doi.org/10.1016/j.ces.2007.02.020>, 2007.
- Sharp, J. H.: Total organic carbon in seawater – comparison of measurements using persulfate oxidation and high temperature combustion, *Mar. Chem.*, 1, 211–229, [https://doi.org/10.1016/0304-4203\(73\)90005-4](https://doi.org/10.1016/0304-4203(73)90005-4), 1973.
- Smichowski, P., Polla, G., and Gómez, D.: Metal fractionation of atmospheric aerosols via sequential chemical extraction: A review, *Anal. Bioanal. Chem.*, 381, 302–316, <https://doi.org/10.1007/s00216-004-2849-x>, 2005.
- Synal, H. A., Stocker, M., and Suter, M.: MICADAS: A new compact radiocarbon AMS system, *Nucl. Instrum. Meth. B*, 259, 7–13, <https://doi.org/10.1016/j.nimb.2007.01.138>, 2007.
- Szidat, S., Jenk, T. M., Gäggeler, H. W., Synal, H.-A., Fisseha, R., Baltensperger, U., Kalberer, M., Samburova, V., Wacker, L., Saurer, M., Schwikowski, M., and Hajdas, I.: Source Apportionment of Aerosols by  $^{14}\text{C}$  Measurements in Different Carbonaceous Particle Fractions, *Radiocarbon*, 46, 475–484, <https://doi.org/10.1017/S0033822200039783>, 2004a.
- Szidat, S., Jenk, T. M., Gäggeler, H. W., Synal, H.-A., Hajdas, I., Bonani, G., and Saurer, M.: THEODORE, a two-step heating system for the EC/OC determination of radiocarbon ( $^{14}\text{C}$ ) in the environment, *Nucl. Instrum. Meth. B*, 223–224, 829–836, <https://doi.org/10.1016/j.nimb.2004.04.153>, 2004b.
- Szidat, S., Jenk, T. M., Synal, H.-A., Kalberer, M., Wacker, L., Hajdas, I., Kasper-Giebl, A., and Baltensperger, U.: Contributions of fossil fuel, biomass-burning, and biogenic emissions to carbonaceous aerosols in Zurich as traced by  $^{14}\text{C}$ , *J. Geophys. Res.*, 111, D07206, <https://doi.org/10.1029/2005JD006590>, 2006.
- Szidat, S., Prévôt, A. S. H., Sandradewi, J., Alfarra, M. R., Synal, H. A., Wacker, L., and Baltensperger, U.: Dominant impact of residential wood burning on particulate matter in Alpine valleys during winter, *Geophys. Res. Lett.*, 34, L05820, <https://doi.org/10.1029/2006GL028325>, 2007.
- Szidat, S., Ruff, M., Perron, N., Wacker, L., Synal, H.-A., Hallquist, M., Shannigrahi, A. S., Yttri, K. E., Dye, C., and Simpson, D.: Fossil and non-fossil sources of organic carbon (OC) and elemental carbon (EC) in Göteborg, Sweden, *Atmos. Chem. Phys.*, 9, 1521–1535, <https://doi.org/10.5194/acp-9-1521-2009>, 2009.
- Szidat, S., Bench, G., Bernardoni, V., Calzolari, G., Czimczik, C. I., Derendorp, L., Dusek, U., Elder, K., Fedi, M. E., Genberg, J., Gustafsson, Ö., Kirillova, E., Kondo, M., McNichol, A. P., Perron, N., Santos, G. M., Stenström, K., Swietlicki, E., Uchida, M., Vecchi, R., Wacker, L., Zhang, Y. L., and Prévôt, A. S. H.: Intercomparison of  $^{14}\text{C}$  analysis of carbonaceous aerosols: Exercise 2009, *Radiocarbon*, 55, 1496–1509, <https://doi.org/10.1017/S0033822200048426>, 2013.
- Szidat, S., Salazar, G. A., Vogel, E., Battaglia, M., Wacker, L., Synal, H.-A., and Türler, A.:  $^{14}\text{C}$  Analysis and Sample Preparation at the new Bern Laboratory for the Analysis of Radiocarbon with AMS (LARA), *Radiocarbon*, 56, 561–566, <https://doi.org/10.2458/56.17457>, 2014.
- Tørseth, K., Aas, W., Breivik, K., Fjæraa, A. M., Fiebig, M., Hjellbrekke, A. G., Lund Myhre, C., Solberg, S., and Yttri, K. E.: Introduction to the European Monitoring and Evaluation Programme (EMEP) and observed atmospheric composition change during 1972–2009, *Atmos. Chem. Phys.*, 12, 5447–5481, <https://doi.org/10.5194/acp-12-5447-2012>, 2012.
- Vlachou, A., Daellenbach, K. R., Bozzetti, C., Chazéau, B., Salazar, G. A., Szidat, S., Jaffrezo, J.-L., Hueglin, C., Baltensperger, U., Haddad, I. E., and Prévôt, A. S. H.: Advanced source apportionment of carbonaceous aerosols by coupling offline AMS and radiocarbon size-segregated measurements over a nearly 2-year period, *Atmos. Chem. Phys.*, 18, 6187–6206, <https://doi.org/10.5194/acp-18-6187-2018>, 2018.

- Wacker, L., Christl, M., and Synal, H. A.: Bats: A new tool for AMS data reduction, *Nucl. Instrum. Meth. B*, 268, 976–979, <https://doi.org/10.1016/j.nimb.2009.10.078>, 2010.
- Wacker, L., Fahrni, S. M., Hajdas, I., Molnar, M., Synal, H. A., Szidat, S., and Zhang, Y. L.: A versatile gas interface for routine radiocarbon analysis with a gas ion source, *Nucl. Instrum. Meth. B*, 294, 315–319, <https://doi.org/10.1016/j.nimb.2012.02.009>, 2013.
- Walker, B. D., Primeau, F. W., Beaupré, S. R., Guilderson, T. P., Druffel, E. R. M., and McCarthy, M. D.: Linked changes in marine dissolved organic carbon molecular size and radiocarbon age, *Geophys. Res. Lett.*, 43, 10385–10393, <https://doi.org/10.1002/2016GL070359>, 2016.
- Weber, R. J., Sullivan, A. P., Peltier, R. E., Russell, A., Yan, B., Zheng, M., de Grouw, J., Warneke, C., Brock, C., Holloway, J. S., Atlas, E. L., and Edgerton, E.: A study of secondary organic aerosol formation in the anthropogenic-influenced southeastern United States, *J. Geophys. Res. Atmos.*, 112, D13302, <https://doi.org/10.1029/2007JD008408>, 2007.
- Wiedemeier, D. B., Lang, S. Q., Gierga, M., Abiven, S., Bernasconi, S. M., Früh-Green, G. L., Hajdas, I., Hanke, U. M., Hilf, M. D., McIntyre, C. P., Scheider, M. P. W., Smittenberg, R. H., Wacker, L., Wiesenberger, G. L. B., and Schmidt, M. W. I.: Characterization, Quantification and Compound-specific Isotopic Analysis of Pyrogenic Carbon Using Benzene Polycarboxylic Acids (BPCA), *J. Vis. Exp.*, 111, e53922, <https://doi.org/10.3791/53922>, 2016.
- Winiger, P., Andersson, A., Yttri, K. E., Tunved, P., and Gustafsson, Ö.: Isotope-Based Source Apportionment of EC Aerosol Particles during Winter High-Pollution Events at the Zeppelin Observatory, Svalbard, *Environ. Sci. Technol.*, 49, 11959–11966, <https://doi.org/10.1021/acs.est.5b02644>, 2015.
- Winiger, P., Andersson, A., Eckhardt, S., Stohl, A., and Gustafsson, Ö.: The sources of atmospheric black carbon at a European gateway to the Arctic, *Nat. Commun.*, 7, 12776, <https://doi.org/10.1038/ncomms12776>, 2016.
- Winiger, P., Andersson, A., Eckhardt, S., Stohl, A., Semiletov, I. P., Dudarev, O. V., Charkin, A., Shakhova, N., Klimont, Z., Heyes, C., and Gustafsson, Ö.: Siberian Arctic black carbon sources constrained by model and observation, *P. Natl. Acad. Sci. USA*, 114, E1054–E1061, <https://doi.org/10.1073/pnas.1613401114>, 2017.
- Winiger, P., Barrett, T. E., Sheesley, R. J., Huang, L., Sharma, S., Barrie, L. A., Yttri, K. E., Evangeliou, N., Eckhardt, S., Stohl, A., Klimont, Z., Heyes, C., Semiletov, I. P., Dudarev, O. V., Charkin, A., Shakhova, N., Holmstrand, H., Andersson, A., and Gustafsson, Ö.: Source apportionment of circum-Arctic atmospheric black carbon from isotopes and modeling, *Sci. Adv.*, 5, eaau8052, <https://doi.org/10.1126/sciadv.aau8052>, 2019.
- Yu, J. Z., Xu, J., and Yang, H.: Charring characteristics of atmospheric organic particulate matter in thermal analysis, *Environ. Sci. Technol.*, 36, 754–761, <https://doi.org/10.1021/es015540q>, 2002.
- Zencak, Z., Elmquist, M., and Gustafsson, Ö.: Quantification and radiocarbon source apportionment of black carbon in atmospheric aerosols using the CTO-375 method, *Atmos. Environ.*, 41, 7895–7906, <https://doi.org/10.1016/j.atmosenv.2007.06.006>, 2007.
- Zenker, K., Vonwiller, M., Szidat, S., Calzolari, G., Giannoni, M., Bernardoni, V., Jedynska, A., Henzing, B., Meijer, H., and Dusek, U.: Evaluation and Inter-Comparison of Oxygen-Based OC-EC Separation Methods for Radiocarbon Analysis of Ambient Aerosol Particle Samples, *Atmosphere (Basel)*, 8, 226, <https://doi.org/10.3390/atmos8110226>, 2017.
- Zhang, Y. L., Liu, D., Shen, C. D., Ding, P., and Zhang, G.: Development of a preparation system for the radiocarbon analysis of organic carbon in carbonaceous aerosols in China, *Nucl. Instrum. Meth. B*, 268, 2831–2834, <https://doi.org/10.1016/j.nimb.2010.06.032>, 2010.
- Zhang, Y. L., Perron, N., Ciobanu, V. G., Zotter, P., Minguilón, M. C., Wacker, L., Prévôt, A. S. H., Baltensperger, U., and Szidat, S.: On the isolation of OC and EC and the optimal strategy of radiocarbon-based source apportionment of carbonaceous aerosols, *Atmos. Chem. Phys.*, 12, 10841–10856, <https://doi.org/10.5194/acp-12-10841-2012>, 2012.
- Zhang, Y.-L., Liu, J., Salazar, G. A., Li, J., Zotter, P., Zhang, G., Shen, R., Schäfer, K., Schnelle-Kreis, J., Prévôt, A. S. H., and Szidat, S.: Micro-scale ( $\mu\text{g}$ ) radiocarbon analysis of water-soluble organic carbon in aerosol samples, *Atmos. Environ.*, 97, 1–5, <https://doi.org/10.1016/j.atmosenv.2014.07.059>, 2014a.
- Zhang, Y. L., Li, J., Zhang, G., Zotter, P., Huang, R. J., Tang, J. H., Wacker, L., Prévôt, A. S. H., and Szidat, S.: Radiocarbon-based source apportionment of carbonaceous aerosols at a regional background site on Hainan Island, South China, *Environ. Sci. Technol.*, 48, 2651–2659, <https://doi.org/10.1021/es4050852>, 2014b.
- Zhang, Y.-L., Huang, R.-J., El Haddad, I., Ho, K.-F., Cao, J.-J., Han, Y., Zotter, P., Bozzetti, C., Daellenbach, K. R., Canonaco, F., Slowik, J. G., Salazar, G., Schwiowski, M., Schnelle-Kreis, J., Abbaszade, G., Zimmermann, R., Baltensperger, U., Prévôt, A. S. H., and Szidat, S.: Fossil vs. non-fossil sources of fine carbonaceous aerosols in four Chinese cities during the extreme winter haze episode of 2013, *Atmos. Chem. Phys.*, 15, 1299–1312, <https://doi.org/10.5194/acp-15-1299-2015>, 2015.
- Zhao, C. and Garrett, T. J.: Effects of Arctic haze on surface cloud radiative forcing, *Geophys. Res. Lett.*, 42, 557–564, <https://doi.org/10.1002/2014GL062015>, 2015.
- Zotter, P., Ciobanu, V. G., Zhang, Y. L., El-Haddad, I., Macchia, M., Daellenbach, K. R., Salazar, G. A., Huang, R.-J., Wacker, L., Hueglin, C., Piazzalunga, A., Fermo, P., Schwiowski, M., Baltensperger, U., Szidat, S., and Prévôt, A. S. H.: Radiocarbon analysis of elemental and organic carbon in Switzerland during winter-smog episodes from 2008 to 2012 – Part 1: Source apportionment and spatial variability, *Atmos. Chem. Phys.*, 14, 13551–13570, <https://doi.org/10.5194/acp-14-13551-2014>, 2014.